Development of alkylated hydrazides as highly potent and selective class I HDAC inhibitors with T cell modulatory properties

Ping Sun[1#], Jing Wang[2#], Khadija Shahed Khan[2], Weiqin Yang[2], Wai-Lung Ng[3], Nikita Ilment[1], Matthes Zessin[1], Emre F. Bülbül[1], Dina Robaa[1], Frank Erdmann[1], Matthias Schmidt[1], Christophe Romier[4], Mike Schutkowski[5], Alfred Sze-Lok Cheng[2*], Wolfgang Sippl[1*].

[1] *Department of Medicinal Chemistry, Institute of Pharmacy, Martin-Luther University of Halle-Wittenberg, 06120 Halle/Saale, Germany*

[2] *School of Biomedical Sciences, The Chinese University of Hong Kong, Hong Kong SAR 999077, China*

[3] *School of Pharmacy, The Chinese University of Hong Kong, Hong Kong SAR 999077, China*

[4] *Université de Strasbourg, CNRS, INSERM, Institut de Génétique et de Biologie Moléculaire et Cellulaire (IGBMC), Département de Biologie Structurale Intégrative, 67404 Illkirch Cedex, France*

[5] *Department of Enzymology, Institute of Biotechnology, Martin-Luther University of Halle-Wittenberg, 06120 Halle/Saale, Germany*

[#]Co-first author

[*]Corresponding authors

Abstract

Histone deacetylases (HDACs) are modulators of epigenetic gene regulation and additionally control the activity of non-histone protein substrates by removing acyl or acetyl groups from modified lysine residues. We recently demonstrated that pharmacological inhibition of the HDAC8 enzyme belonging to class I of HDACs and overexpressed in a variety of human cancers controls histone H3 lysine 27 (H3K27)-acetylation and reduces hepatocellular carcinoma tumorigenicity in a T cell-dependent manner. Here, we present a new chemotype of alkylated hydrazide-based class I HDAC inhibitors in which the *n*-hexyl side chain attached to the hydrazide moiety show HDAC8 selectivity *in vitro*. An enzymatic assay provided important structure-activity relationships for this new series of alkyl hydrazides. Analysis of the mode of inhibition of the alkyl hydrazides against HDAC8 revealed a substrate-competitive binding mode. The most promising compound **7d** marked induced acetylation of the HDAC8 substrates H3K27 and SMC3 at 10 μM but not tubulin in $CD4^+$ T lymphocytes, and significantly upregulated gene expressions for memory and effector functions. Furthermore, intraperitoneal injection administration of **7d** (10 mg/kg) in C57BL/6 mice increased *interleukin-2* expression in $CD4^+$ T cells and $CD8^+$ T cell proportion with no apparent toxicity. This study expands a novel chemotype of highly potent class I HDAC inhibitors with T cell modulatory properties for future therapeutic applications.

Introduction

Histone deacetylases (HDACs) are a family of enzymes that catalyze the removal of acetyl or acyl groups from the modified ε-amino moiety of lysine in histone tails resulting in the compaction of chromatin and the subsequent gene transcriptional

repression.[1-2] In addition, more and more non-histone proteins have been reported as substrates.[3] 18 HDAC subtypes have been identified and grouped into four different classes based on their architecture and sequence homology to yeast HDAC proteins. Zinc-dependent HDACs are grouped into class I (HDAC1, 2, 3, HDAC8), class IIa (HDAC4, 5, HDAC7, HDAC9), IIb (HDAC 6 and HDAC10) and class IV (HDAC11). Meanwhile, the catalytic activity of class III HDACs, classically termed as sirtuins (Sirt1-7), is initiated by nicotinamide adenine dinucleotide (NAD^+). Class I HDACs (HDAC1-3, HDAC8) are ubiquitously expressed and mainly located in the nucleus. HDAC8 can conduct its catalytic functions without protein partners while HDAC1-3 generally form large protein complexes with each other and co-repressor proteins to control their enzymatic activities.[1, 4] Both histone and non–histone proteins such as AMP-activated protein kinase, structural maintenance of chromosomes protein 3 (SMC3) and p53 were identified as substrates of class I HDACs.[5]

Class I HDACs have been extensively investigated and linked to diverse haematological malignancies,[6-8] and solid tumors, including colon cancer,[9] lung cancer,[10] pancreatic cancer,[11] neuroblastoma,[12-14] hepatocellular carcinoma (HCC),[15-16] T-cell lymphomas[17] and multiple myeloma,[18] as well as neurodegenerative diseases like Alzheimer's disease.[19] In addition, an impact on immune dysfunction diseases such as HIV infection,[20] metabolic disorders,[21] inflammatory diseases has been reported.[22] Therefore, using histone deacetylases inhibitors (HDACi) to regulate the hyperacetylation status of histone and non-histone proteins can lead to therapeutic outcomes by influencing cellular pathways in all phases of the aberrant cells' lifetime, inducing tumor suppressors or modulating the immune response.[6, 23-26] Based on this, considerable progress has been achieved during the past three decades to develop HDAC inhibitors as therapeutic agents with pan-HDAC inhibitors including

vorinostat, romidepsin, belinostat, and panobinostat as well as the class I inhibitor chidamide being approved for the treatment of T-cell lymphomas and multiple myeloma and numerous other HDAC inhibitors currently in various stages of clinical trials.[27]

HDAC inhibitors generally display a canonical pharmacophore model (using PCI-34051[28] as reference, Figure 1): a zinc binding group (ZBG) to chelate the catalytic zinc ion on one side and a capping group binding to the rim of the protein on the other side, both of them are connected with a linker group to occupy the HDAC hydrophobic channel. To date, hydroxamic acids and aminobenzamides are the most frequently used ZBGs both in clinically approved drugs and in the undergoing HDAC inhibitor development practice. However, therapeutic efficacies of hydroxamic acid or aminobenzamide containing HDAC inhibitors were influenced by dose-limiting toxicities and off-target effects[29] due to several factors including poor selectivity profiles over certain related metalloproteins as well as other zinc-dependent HDAC subtypes, chemical stability problems, sulfation and glucuronidation-based metabolic inactivation, and mutagenic effects.[30-33] Accordingly, other novel ZBG-based HDAC inhibitor discovery has recently drew great attention with the aspiration to overcome these shortcomings of hydroxamic acid and aminobenzamide-based HDAC inhibitors.[27] In addition, capping group modification represents another promising approach to increase the selectivity profile of HDAC inhibitors to reduce off-target effects.[34]

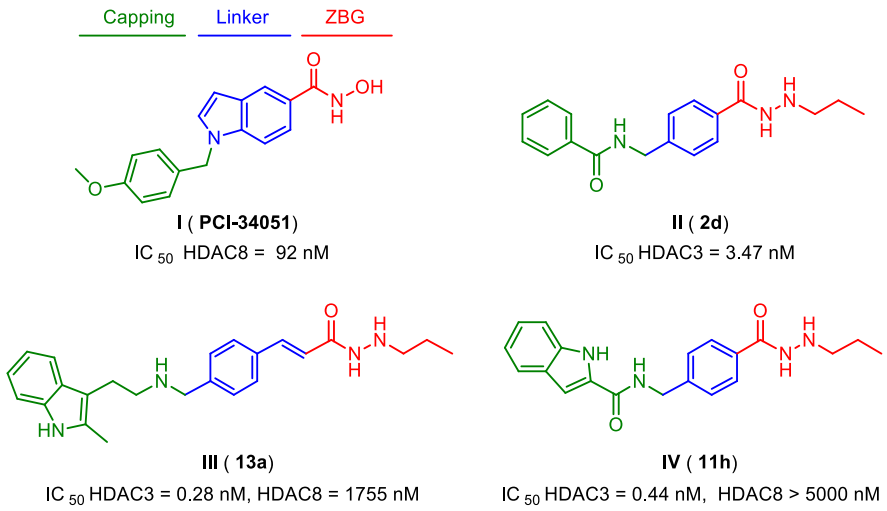

Figure 1. Structures of reported alkylated hydrazide based HDAC inhibitors as well as the HDAC8 reference inhibitor PCI-34051.

In recent years, hydrazides incorporating an *n*-propyl or *n*-butyl side chain have been described as novel HDAC3 inhibitors with *in vitro* and *in vivo* efficacy for acute myeloid leukemia.[35-40] Several of them exhibited good oral bioavailability and good pharmacokinetic profiles. Importantly, these series of compounds are more stable and bioavailable compared to their hydroxamic acid-based parent HDAC inhibitors[40] (Figure 1). For example: compound **II** was reported as a metabolic stable inhibitor confirmed by ESI-LC/MS experiments.[37] Compound **III** not only displayed a better mutagenic profile than panobinostat in a primary Ames test, but also possessed a good pharmacokinetic profile in mice (oral bioavailability: F% = 19.8%).[39] Further, compound **IV** was identified as a more effective class I HDAC inhibitor than panobinostat in *in vitro* and *in vivo* antitumor activity studies and demonstrated an excellent pharmacokinetic/pharmacodynamics profile (oral bioavailability: F% = 112%).[35] Beyond the canonical HDACi pharmacophore model parts, the alkyl side chains of these hydrazides are thought to be accommodated in the hydrophobic "foot-pocket" which is a conserved structural feature of class I HDACs.[3, 34, 36, 41]

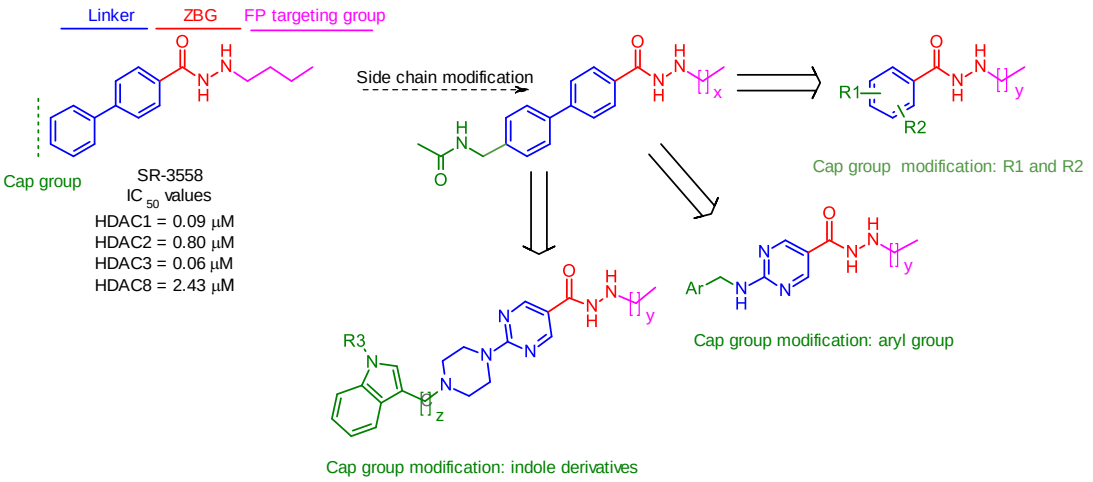

Figure 2. Design strategy: x = 2 -5; y = 2 or 5; z = 1 or 2; R_1 = methyl or H; R_2 = phenyl or benzylamino; R_3 = methyl or H.

SR-3558 was recently reported as class I HDAC1/3 inhibitor (IC_{50} = 0.09 µM and 0.06 µM against HDAC1 and HDAC3 respectively, Figure 2) which was additionally used for the development of HDAC3 specific proteolysis targeting chimera (PROTAC).[42]

In this work, we set to introduce various structural modifications on alkylhydrazides as lead structures in order to explore their impact on the selectivity profile against different HDAC subtypes as well as attempt to generate cellular active compounds. To this end, the foot-pocket targeting group was altered by modifying the length of the alkyl side chain attached to the hydrazide moiety. Further modifications included the introduction of a phenyl, an aminopyrimidine or a piperazinyl-pyrimidine moiety as linker group and benzylamines or indole derivatives as cap groups (Figure 2). All compounds were first tested using an *in vitro* enzymatic assay and the results provided important structure-activity relationships for this class of inhibitors. As we have recently demonstrated potent T cell memory response by combined HDAC8 inhibition and immune-checkpoint blockade in hepatocellular carcinoma (HCC) therapy,[16] target engagement of the new compounds was studied by means of western

blots in Jurkat T lymphocytes and the best candidates were further investigated by gene expression for T cell functions. The most promising HDAC8 inhibitor was used for functional characterization in naïve mice analyzing the T cell modulatory effects.

Chemistry

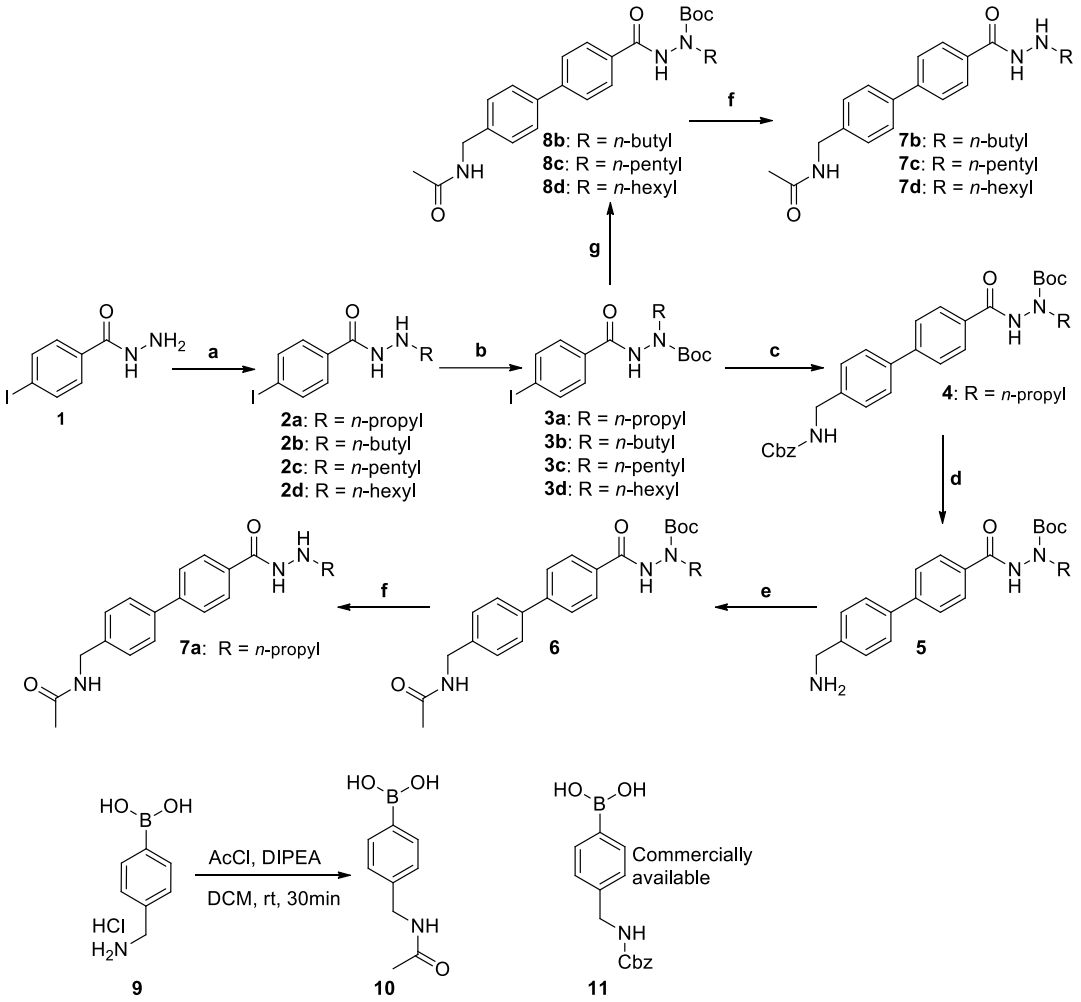

Scheme 1. Reagents and conditions: (a) Aldehyde 1.05 eq, pTSA 0.05 eq, MeOH, rt, 2 h, then $NaBH(AcO)_3$ 2.0 eq, 1 h, rt; (b) $(Boc)_2O$ 1.1 eq; TEA 2.5 eq, THF, rt; (c) **11** 1.0 eq, $Pd(PPh_3)_4$ 0.04 eq, K_2CO_3 2.5 eq, PhMe/MeOH/H_2O, 90 °C, 7 h; (d) Pd/C (10%), $NaBH_4$ 5.0 eq, MeOH, overnight; (e) AcCl 1.5 eq, DIPEA 3.0 eq, DCM, rt, 30 min; (f) HCl/dioxane, DCM, rt, 3 h; (g) **10** 1.0 eq, $Pd(PPh_3)_4$ 0.04 eq, K_2CO_3 2.5 eq, PhMe/MeOH/H_2O, 90 °C, 7 h.

In the first series of compounds, the *N*-protected boronic acid key intermediates **10** and **11** were either attained through commercial sources (Cbz (benzyl chlorocarbonate) protected compound **11**) or via acetylation of 4-(aminomethyl)phenylboronic acid (**9**) (Scheme 1). In the subsequent procedures, *N*-alkyl groups of different lengths were introduced to 4-iodobenzohydrazide (**1)** via a one pot reaction with different aldehydes followed by hydrogenation using $NaBH(AcO)_3$. The corresponding products **2a-d** were protected with Boc, then coupled with boronic acid through Suzuki coupling. A subsequent Boc-deprotection afforded the final biphenyl products **7b-d**. To attain the derivative **7a**, the boronic acid derivative **11** was coupled with the intermediate compound **3a**, and the obtained product was Cbz-deprotected to generate intermediate **5**. The latter compound was subjected to an acetylation step and a subsequent Boc-deprotection to yield **7a**.

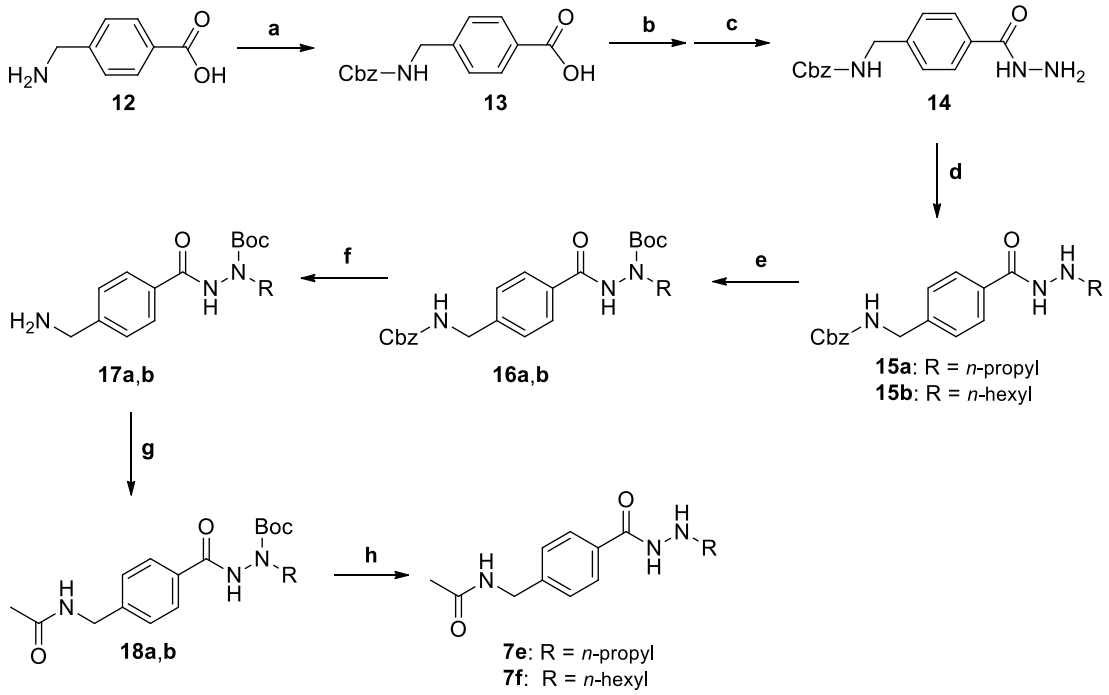

Scheme 2. Reagents and conditions: (a) CbzCl 1.1 eq, Na_2CO_3 4.0 eq, H_2O, ice bath to rt, 1.5 h; (b) CDI 1.05 eq, THF, 30 min; (c) hydrazine monohydate 10.0 eq, THF, rt; (d) Aldehyde 1.1 eq, $NaBH(AcO)_3$ 3.0 eq, DCM, rt, overnight or aldehyde 1.05 eq, pTSA 0.05 eq, MeOH, 2 h, then $NaBH_4$ 4.0 eq, 1 h; (e) $(Boc)_2O$ 1.1 eq; TEA 2.5 eq, THF, rt; (f) Pd/C (10%), $NaBH_4$ 5.0 eq, MeOH, rt, overnight; (g) AcCl 1.5 eq, DIPEA 3.0 eq, DCM, rt; (h) HCl/dioxane, DCM, rt, 3 h.

For the second series, the starting 4-(aminomethyl)benzoic acid (**12**) was protected by the basic condition stable Cbz group, then condensed with hydrazine hydrate to afford compound **14**. Subsequently, similar steps as adapted for the synthesis of compound **7a** were implemented to give **7e** and **7f** (Scheme 2).

The target hydrazide derivatives **7g** and **7h** were easily synthesized starting from the respective ethyl 3-aminobenzoates **19a,b** which were first benzylated then converted to the respective hydrazides and finally converted to the N-alkylated hydrazide derivatives as shown in Scheme 3.

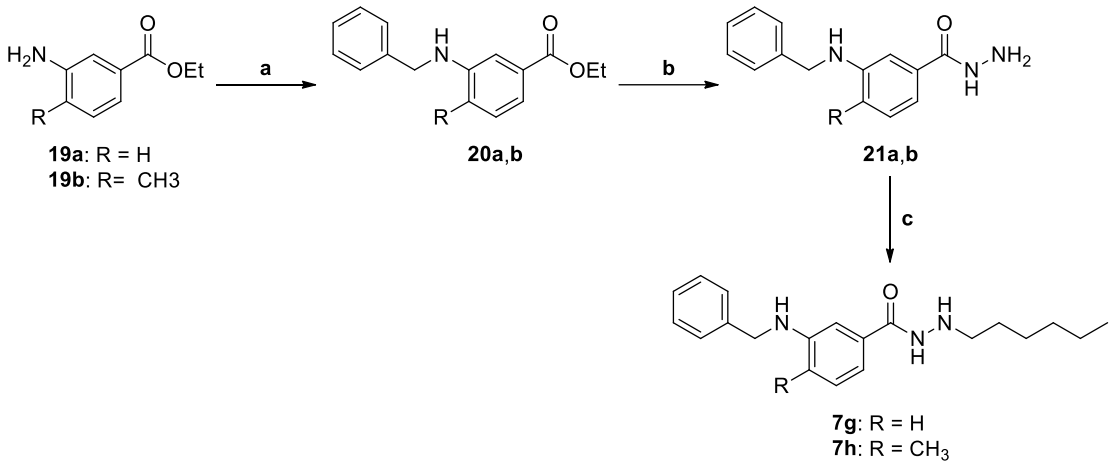

Scheme 3. Reagents and conditions: (a) benzyl chloride, K_2CO_3, DMF; (b) hydrazine monohydrate 10.0 eq, EtOH, microwave 110 ^oC, 1 h; (c) hexanal 1.05 eq, pTSA 0.05 eq, MeOH, 2 h, then $NaBH_4$ 4.0 eq, 1 h.

For the pyrimidine analogs **28a-m,** ethyl 2-chloropyrimidine-4-carboxylate (**25**) was used as starting material. A nucleophilic aromatic substitution reaction with the respective amine followed by hydrazine acylation afforded the intermediate **27a-m**. The latter were finally transformed into the alkylated products **28a-m**. The key intermediate amine **24** for attaining compounds **28i** and **28m** was prepared from starting material **22** (Scheme 4).

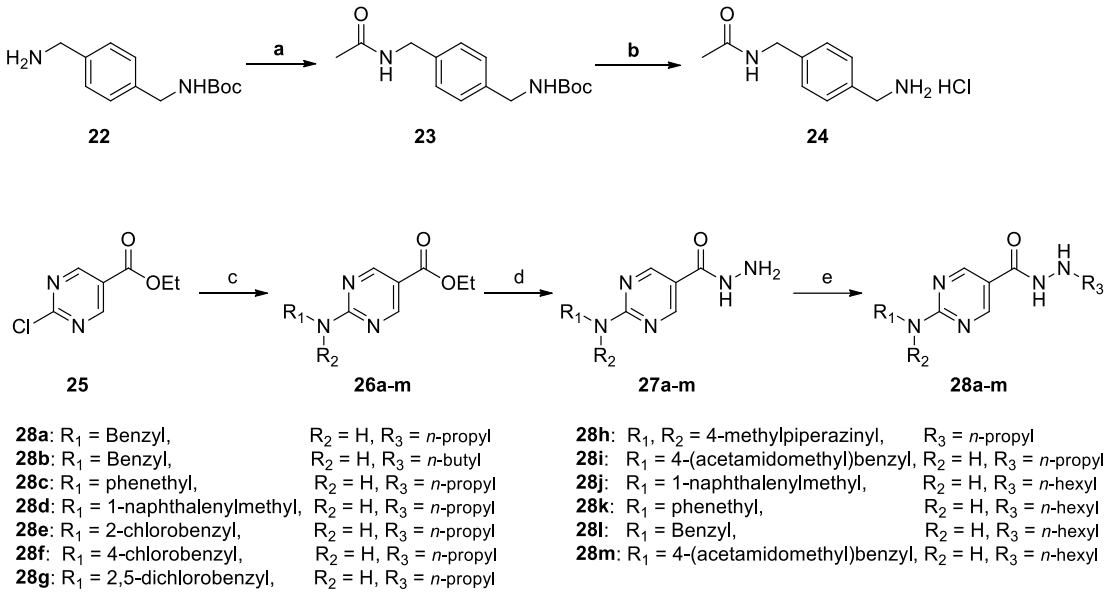

28a: R_1 = Benzyl, R_2 = H, R_3 = *n*-propyl
28b: R_1 = Benzyl, R_2 = H, R_3 = *n*-butyl
28c: R_1 = phenethyl, R_2 = H, R_3 = *n*-propyl
28d: R_1 = 1-naphthalenylmethyl, R_2 = H, R_3 = *n*-propyl
28e: R_1 = 2-chlorobenzyl, R_2 = H, R_3 = *n*-propyl
28f: R_1 = 4-chlorobenzyl, R_2 = H, R_3 = *n*-propyl
28g: R_1 = 2,5-dichlorobenzyl, R_2 = H, R_3 = *n*-propyl

28h: R_1, R_2 = 4-methylpiperazinyl, R_3 = *n*-propyl
28i: R_1 = 4-(acetamidomethyl)benzyl, R_2 = H, R_3 = *n*-propyl
28j: R_1 = 1-naphthalenylmethyl, R_2 = H, R_3 = *n*-hexyl
28k: R_1 = phenethyl, R_2 = H, R_3 = *n*-hexyl
28l: R_1 = Benzyl, R_2 = H, R_3 = *n*-hexyl
28m: R_1 = 4-(acetamidomethyl)benzyl, R_2 = H, R_3 = *n*-hexyl

Scheme 4. Reagents and conditions: (a) AcCl 1.5 eq, DIPEA 3.0 eq, DCM, 30 min; (b) HCl/dioxane, DCM, rt, 3 h; (c) **24** or R_1R_2NH 1.0 eq, DIPEA 3.5 (for **24**) or 2.5 eq, DCM, rt, 0.5 to 3 h; (d) hydrazine monohydate 30.0 eq, EtOH, reflux, 0.5 to 3 h or hydrazine monohydate 10.0 eq, EtOH, microwave 110 ^{o}C, 1 h; (e) aldehyde 1.05 eq, pTSA 0.05 eq, MeOH, 2 h, then $NaBH_4$ 4.0 eq, 1 h.

The final series of derivatives bearing a piperazine moiety attached to the pyrimidine linker and indole capping groups (Scheme 5) were synthesized as follows. Mono-*N*-benzylpiperazine was synthesized and coupled with the pyrimidine moiety of compound **25** in a nucleophilic aromatic substitution reaction. The corresponding product **34** was converted to the hydrazide **35** which was subjected to subsequent alkylation, Boc-protection and benzyl removal to afford the key intermediate **38**. The latter compound was ultimately transformed to the designed compounds **40a-e** through reductive amination or nucleophilic substitution reaction with different indole derivatives.

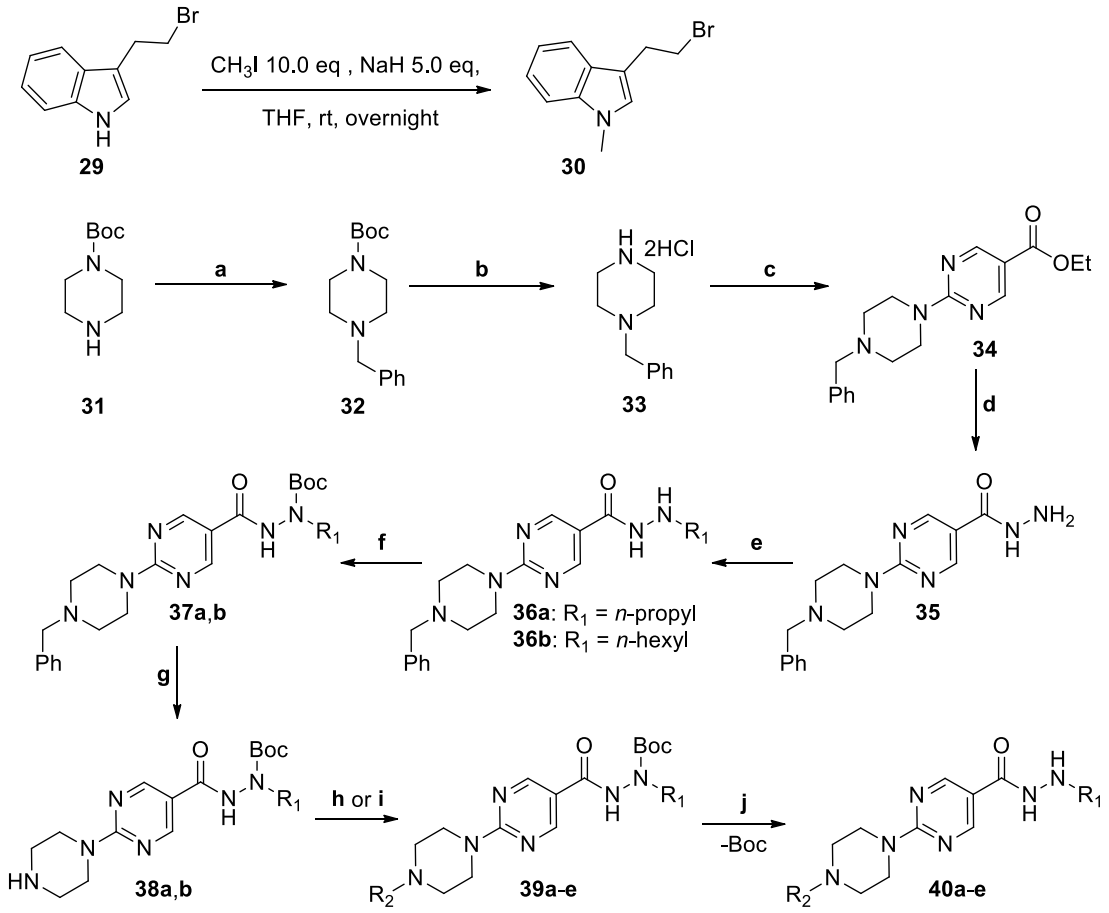

Scheme 5. Reagents and conditions: (a) benzyl chloride 2.0 eq, K_2CO_3 5.8 eq, EtOH, reflux, overnight; (b) HCl/Dioxane, DCM, rt, 3 h; (c) **25** 1.0 eq, DIPEA 4.5 eq, DCM, rt, 1 h; (d) hydrazine monohydrate 30.0 eq, EtOH, reflux; (e) aldehyde 1.05 eq, pTSA 0.05 eq, MeOH, 2 h, then $NaBH_4$ 4.0 eq, 1 h; (f) $(Boc)_2O$ 1.1 eq, TEA 2.5 eq, DCM, rt, overnight; (g) Pd/C (10%), ammonium formate 4.0 eq, EtOH, 60 °C, 4 h; (h) aldehyde 1.0 eq, $NaBH(AcO)_3$ 2.0 eq, DCM, rt, overnight; (i) alkyl bromide 1.2 eq, K_2CO_3 2.5 eq, DMF, 80 °C, overnight; (j) HCl/dioxane, DCM, ice bath, 3 h.

Structure-activity relationships

Table 1. *In vitro* HDAC inhibitory activity of first series of biphenyl containing alkylhydrazides.

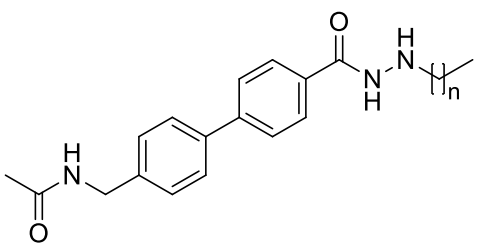

Cpd No.	n	IC_{50} in μM			
		HDAC1	HDAC2	HDAC3	HDAC8
7a	2	1.6 ± 0.1	0.63 ± 0.03	0.091 ± 0.003	0.7 ± 0.07
7b	3	0.62 ± 0.05	1.1 ± 0.1	0.35 ± 0.02	0.36 ± 0.02
7c	4	0.66 ± 0.05	2.0 ± 0.2	1.5 ± 0.1	0.35 ± 0.01
7d	5	1.8 ± 0.3	12 ± 1	>20	0.036 ± 0.002

In the first series of inhibitors an acetamidomethyl group was attached as terminal group. Docking studies (discussed in details later) revealed that this group is able to form a hydrogen bond with an aspartate residue (Asp101 in HDAC8 and Asp93 in HDAC3) in the peripheral region of different HDAC subtypes. The impact of the length of the alkyl group attached to the hydrazide moiety was tested by using a chain length between 3 and 6 carbon atoms. All synthesized compounds were measured using a recently developed fluorescence-based activity assay using recombinant class I HDAC (HDAC1, -2. -3, -8) proteins.[43-44] As observed in previous studies, the *n*-propyl derivative **7a** showed an IC_{50} of 0.091 μM towards HDAC3 and improved selectivity profiles over HDAC1 and HDAC8 (IC_{50} = 1.6 μM and 0.7 μM, respectively; Table 1) compared to the parent compound SR-3558. Surprisingly, the *n*-hexyl derivative **7d** showed potent HDAC8 inhibition (IC_{50} = 36 nM) and selectivity over the other tested HDAC subtypes. Derivatives bearing *n*-butylated or *n*-pentylated hydrazide moieties showed moderate activities towards all tested HDAC-isoforms without apparent selectivity. This indicates that alkyl groups of 3 (**7a**) and 6 carbon length (**7d**) possess the ideal size to occupy the hydrophobic foot-pocket in HDAC3 and HDAC8, respectively.

Table 2. *In vitro* HDAC inhibitory activity of phenyl substituted derivatives.

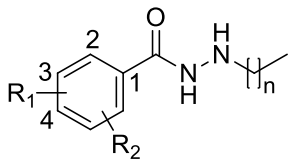

Cpd No.	3-R_1	4-R_2	n	IC_{50} in µM (or % inhibition)			
				HDAC1	HDAC2	HDAC3	HDAC8
7e	H		2	1.6 ± 0.2	5.5 ± 0.4	1.6 ± 0.1	n.d.
7f	H		5	4.8 ± 0.4	12 ± 1	> 20	0.023 ± 0.001
7g	benzylamino	H	5	> 20	> 20	> 20	0.046 ± 0.003
7h	benzylamino	CH_3	5	9% @1 µM 35% @10 µM	5% @1 µM 26% @10 µM	9% @1 µM 42% @10 µM	2% @1 µM 100% @10µM

In the following steps, the cap group of the potent HDAC3 and HDAC8 selective inhibitors **7a** and **7d** was modified by truncating one phenyl ring of the biphenyl core leading to compounds **7e** and **7f**. Additionally, the acetamidomethyl capping group at position 4 of the phenyl linker moiety was replaced by a benzylamino group in position 3 resulting in compounds **7g** and **7h,** the latter bears an additional methyl group at position 4. These derivatives resemble previously developed hydroxamic acid based HDAC8 inhibitors (Table 2).[13] The inhibitory activity of **7e** on HDAC3 (IC_{50} = 1.6 µM) showed a significant decrease when compared to **7a**. Meanwhile the *n*-hexyl derivative **7f** exhibited a slightly improved inhibitory activity towards HDAC8 (IC_{50} = 23 nM) when compared to its counterpart **7d**. Replacing the acetamidomethyl capping group of **7f** with an *N*-benzylamino group at position 3 resulted in compound **7g** with an even superior selectivity for HDAC8, coupled with a significant loss in activity on HDAC1-3. An additional methyl substituent at position 4 (compound **7h**), however, was not well tolerated and resulted in a loss of HDAC8 inhibitory activity (Table 2).

Table 3. *In vitro* HDAC inhibitory activity of of 2-aminopyrimidine derivatives.

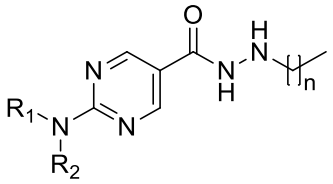

Cpd No.	R_1	R_2	n	IC_{50} in µM (or % inhibition)			
				HDAC1	HDAC2	HDAC3	HDAC8
28a		H	2	0.25 ± 0.02	0.7 ± 0.03	0.043 ± 0.005	1.0 ± 0.11
28b		H	3	61% @1 µM 85% @10 µM	46% @1 µM 93% @10 µM	0.20 ± 0.01	66% @1 µM 94% @10 µM
28c		H	2	51% @1 µM 85% @10 µM	39% @1 µM 90% @10 µM	41% @1 µM 87% @10 µM	51% @1 µM 89% @10 µM
28d		H	2	53% @1 µM 91% @10 µM	46% @1 µM 93% @10 µM	0.081 ± 0.002	36% @1 µM 83% @10 µM
28e		H	2	71% @1 µM 89% @10 µM	55% @1 µM 92% @10 µM	0.060 ± 0.001	43% @1 µM 87% @10 µM
28f	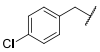	H	2	54% @1 µM 92% @10 µM	61% @1 µM 96% @10 µM	0.037 ± 0.001	62% @1 µM 88% @10 µM
28g		H	2	66% @1 µM 88% @10 µM	n.d.	0.058 ± 0.002	33% @1 µM 83% @10 µM
28h		-	2	0.59 ± 0,03	2.4 ± 0.1	0.12 ± 0.01	0.25 ± 0.01
28i	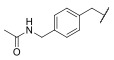	H	2	0.29 ± 0.02	0.92 ± 0.04	0.11 ± 0.01	n.d
28j		H	5	8.3 ± 1.2	> 20	> 20	0.063 ± 0.004
28k		H	5	2.2 ± 0.1	12 ± 1	7.2 ± 0.2	0.028 ± 0.002
28l		H	5	0.56 ± 0.03	3.2 ± 0.2	3.0 ± 0.2	0.016 ± 0,001
28m	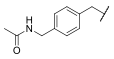	H	5	0.96 ± 0.06	4.5 ± 0.3	8.5 ± 0.4	0.019 ± 0.001

In the next series, the phenyl or biphenyl linkers were replaced by an aminopyrimidine group, while different *N*-arylmethyl, *N*-arylethyl or *N*-

methylpiperazinyl moieties were applied as capping group to yield compounds **28a-m** (Table 3). Within the series of *N*-propylhydrazide derivatives, all compounds bearing substituted or unsubstituted benzyl capping groups showed nanomolar inhibitory activities towards HDAC3 and selectivity over other tested HDAC subtypes. The para-chlorobenzyl derivative **28f** showed the most potent HDAC3 activity (IC_{50} = 37 nM) among this series of compounds. Consistent with our findings regarding the biphenyl scaffold series, the *N*-butylhydrazide derivative **28b** showed a significant decrease in HDAC3 inhibitory activity. Meanwhile, all *N*-hexylhydrazide derivatives, bearing substituted aryl cap groups demonstrated nanomolar inhibitory potency with good selectivity towards HDAC8. These findings support our previous observations that *n*-propyl and *n*-hexyl groups are ideal matches for the foot-pocket of HDAC3 and HDAC8, respectively.

Table 4. *In vitro* HDAC inhibitory activity of piperazinyl-pyrimidine derivatives.

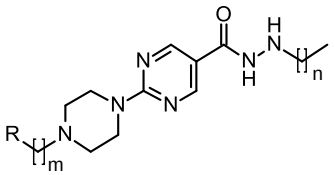

Cpd No.	R	n	m	IC_{50} in μM			
				HDAC1	HDAC2	HDAC3	HDAC8
40a		2	1	0.073 ± 0.007	1.1 ± 0.1	0.030 ± 0.001	0.0082 ± 0.0006
40b		5	1	0.17 ± 0.01	0.31 ± 0.01	0.10 ± 0.04	0.0059 ± 0.0006
40c		5	1	0.17 ± 0.01	0.33 ± 0.02	0.30 ± 0.02	0.014 ± 0.001
40d		5	2	0.86 ± 0.07	1.40 ± 0.10	1.00 ± 0.10	0.013 ± 0.001
40e		5	2	0.46 ± 0.03	1.20 ± 0.10	1.40 ± 0.10	0.023 ± 0.002

In the last series, indole and *N*-methylindole groups were attached via one or two carbon linkers to the piperazinyl-pyrimidine moiety (**40a-e**; Table 4). Interestingly, all compounds showed the most pronounced inhibitory activity on HDAC8, all in the nanomolar range, even for the *N*-propylhydrazide derivative **40a**. Nanomolar to submicromolar inhibitory potency was also observed on HDAC11. The strongest HDAC8 inhibitory activity was displayed by compound **40b** (IC_{50} = 5.9 nM against HDAC8) which also showed significant activity against HDAC11 (IC_{50} = 40 nM).

Selectivity profile of representative compounds

To further study the selectivity profiles of the developed alkylated hydrazides-based inhibitors towards other HDAC subtypes, most potent inhibitors (HDAC3 selective inhibitors **7a**, **28a** and **40a** as well as the HDAC8 selective inhibitors **7d**, **7g** and **40b)** were also tested against class IIa (HDAC4), class IIb (HDAC6) and class IV (HDAC11) enzymes (Table 5). As references we included the reported HDAC8 selective inhibitor PCI34051, the HDAC3 reference inhibitor RGFP966 as well as the HDAC11 selective inhibitor SIS117[45]. All synthesized alkylhydrazide-based inhibitors exhibit no inhibition against HDAC4 and HDAC6 except for **7a** which showed an IC_{50} = 0.99 μM for HDAC4. In case of the highly active HDAC8 inhibitor **40b** also a strong HDAC11 inhibition, comparable to the potency of SIS17, was measured.

Table 5. *In vitro* selectivity profile of selected HDAC inhibitors.

Cpd No.	IC_{50} in μM						
	HDAC1	HDAC2	HDAC3	HDAC8	HDAC4	HDAC6	HDAC11
7a	1.6 ± 0.1	0.63 ± 0.03	0.091 ± 0.003	0.7 ± 0.07	0.99	> 20	1.8 ± 0.2
7d	1.8 ± 0.3	12 ± 1	> 20	0.036 ± 0.003	> 20	> 20	0.18 ± 0.02

7g	> 20	> 20	> 20	0.046 ± 0.003	> 20	> 20	8.6 ± 1.1
28a	0.25 ± 0.02	0.7 ± 0.03	0.043 ± 0.005	1.0 ± 0.11	> 20	> 20	2.0 ± 0.2
40a	0.073 ± 0.007	1.1 ± 0.1	0.030 ± 0.001	0.0082 ± 0.0006	>20	>20	0.570 ± 0.03
40b	0.17 ± 0.01	0.31 ± 0.01	0.10 ± 0.04	0.0059 ± 0.0006	> 20	> 20	0.041 ± 0.003
PCI34051	28.3 ± 2.0[a]	>20	>20	0.092 ± 0.015[a]	>20	48.2 ± 6.2	1.7 ± 0.1
SIS117	>20	>20	>20	12.3 ± 1.1	>20	>20	0.063 ± 0.004
RGFP966	16 ± 2	11 ± 1	1.3 ± 0.1	n.d.	n.d.	n.d.	n.d.

Analysis of type of inhibition

In a next step we studied the mode of action of the developed HDAC8 inhibitors. For this purpose we started with competition experiments. As HDAC8 substrate the recently developed peptide Abz-SRGGK(STFA)FFRR-NH_2 (S) was used in different concentrations to determine the HDAC8 K_i values for two potent inhibitors, namely **7d** and **40a**. A Lineweaver-Burk plot was generated based on the measured enzyme kinetics to predict the inhibition type and the K_i values of the two selected compounds

(Figure 3).

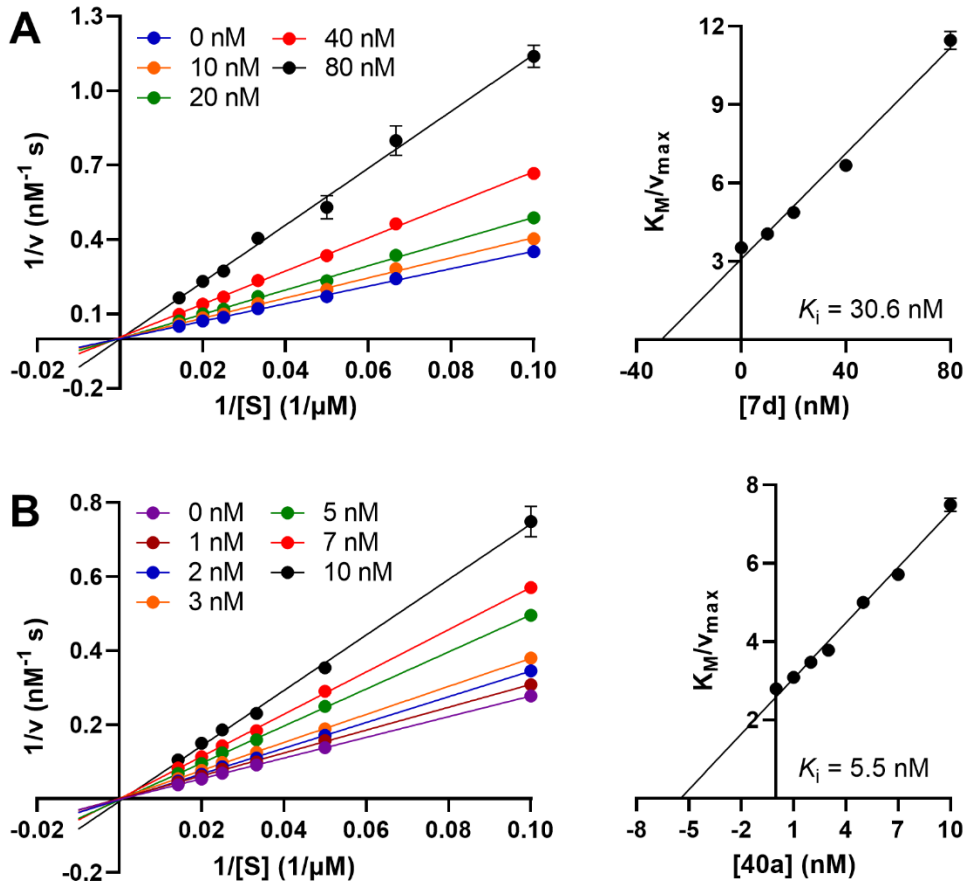

Figure 3. Different Lineweaver-Burk and tertiary plots of enzyme kinetics data of HDAC8 for **7d** (A) and **40a** (B). As substrate the peptide Abz-SRGGK(STFA)FFRR-NH_2 was used with concentrations ranging from 5 to 70 µM whereas the HDAC8 concentration was set to 2 nM. Y-axes units left: $(nM^{-1}\ s))^{-1}$, x-axes units: (μM^{-1}) for HDAC8.

Table 6. Calculated K_i values for HDAC8 by Lineweaver-Burk plots

Inhibitors	K_i (nM)
7d	30.6
40a	5.5

The measured K_i values of the two inhibitors were found to be in good agreement with the obtained IC_{50} values. From the observed characters of the plots, we can

conclude that **7d** and **40a** are both substrate competitive inhibitors against HDAC8 (lines for different substrate concentrations intersect at the origin on the x-axis).

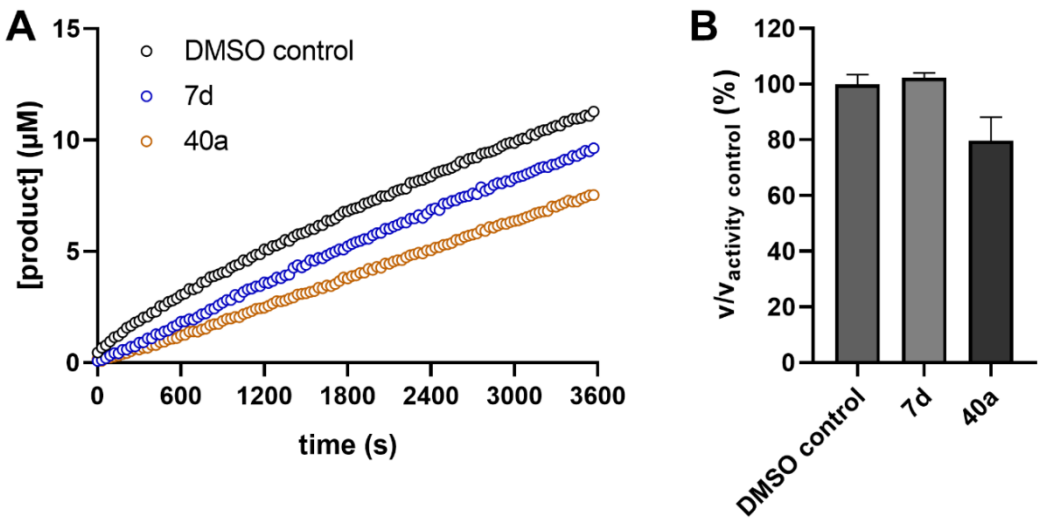

Figure 4: Test of binding reversibility of **7d** and **40a** to HDAC8. A jump dilution experiment was done to examine the reversibility of the inhibition of compounds **7d** and **40a**. (**A)** Inhibitor concentration 10 times higher than the IC_{50} was incubated with 100-fold concentrated enzyme in assay buffer for 30 min at room temperature. The mixture was then rapidly diluted 1:100 with a substrate solution and the product (acetylated peptide) formation was monitored by measuring the change of the fluorescence intensity. (**B)** HDAC8 activity of the jump dilution experiment relative to the control with the same experimental conditions but without the dilution jump. Activity of HDAC8 was completely retained after incubation with **7d** and after the jump dilution. In the case of **40a**, 80% activity was retained after jump dilution.

To test the binding reversibility of the compounds **7d** and **40a,** a jump dilution test based on the HDAC8 activity assay described above was used (details see Methods section). The test showed that both inhibitors are reversibly binding to HDAC8 (Figure 4).

Docking studies

To analyze the HDAC binding mode of the synthesized compounds and to rationalize the observed selectivity, molecular docking studies were performed using the available crystal structures of HDAC1 (PDB ID: 4BKX), HDAC2 (PDB ID: 4LXZ), HDAC3 (PDB ID: 4A69), HDAC6 (PDB ID: 5EDU), and HDAC8 (PDB ID: 1T69).

In the case of the first series, we observed a similar binding pose for **7a-c** in HDAC1-3 and HDAC8 as exemplified by the docking poses of **7a** (Figure 5). The methyl acetamide cap group is solvent-exposed and accommodated at the surface while making hydrogen bond interactions with the conserved aspartate (D93/101 in HDAC3/8, respectively). The biphenyl linker group is sandwiched between two phenylalanine residues (F144/152 and F200/208 in HDAC3/8, respectively) by exhibiting pi-pi interactions in the hydrophobic tunnel. The hydrazide zinc binding group showed a bidentate chelation pattern with the catalytic zinc ion and is engaged in hydrogen bond interactions with H134/142, H135/143 and Y298/306 at the catalytic region in HDAC3/8, respectively (Figure 5A/B). Meanwhile, the *N*-alkyl chain with different lengths showed differences which might explain the selectivity for HDAC3 and HDAC8. It can be observed that the *n*-propyl chain of **7a** perfectly fits into the foot-pocket region of HDAC3 compared to HDAC1/2/8. It's worth noting that the foot-pocket of HDAC3 is narrower than that of HDAC1/2 due the presence of the bulkier Y107 in HDAC3 (replaced by S113/118 in HDAC1/2, respectively) which pushes L133 in HDAC3 (L139/144 in HDAC1/2, respectively) deeper into the foot-pocket resulting in its narrowing (Figure S1A/B, Supplement). Hence, the *n*-butyl, *n*-pentyl and *n*-hexyl chains of **7b, 7c** and **7d**, respectively, are not well accommodated in the HDAC3-foot-pocket and are clashing with the side chains of M24, R28 and L133 in HDAC3 resulting in decrease or loss of HDAC3 activity due to this steric hindrance observed in HDAC3 (Figure 5C). On the other hand, the HDAC8 foot-

pocket is significantly different in shape and size (Figure S1B, Supplement). L133 in HDAC3 is replaced by the bulky W141 in HDAC8. In addition, replacing M24 in HDAC3 with I34 results in a larger foot-pocket size in HDAC8. Thus, **7d** is able to well accommodate into the foot-pocket of HDAC8 by interacting with I34 and W141 which might be the reason for the observed high HDAC8 inhibitory activity and selectivity (Figure 5D). Meanwhile, **7a** and **7d** were docked to the HDAC6 which is one of the class IIb HDAC members. Since HDAC6 does not possess a foot-pocket region and the active sites shows a different shape, both compounds did not show a reasonable binding pose and the hydrazide moiety was not able to chelate the catalytic zinc ion (shown for **7a** as example in Figure S2C, Supplement).

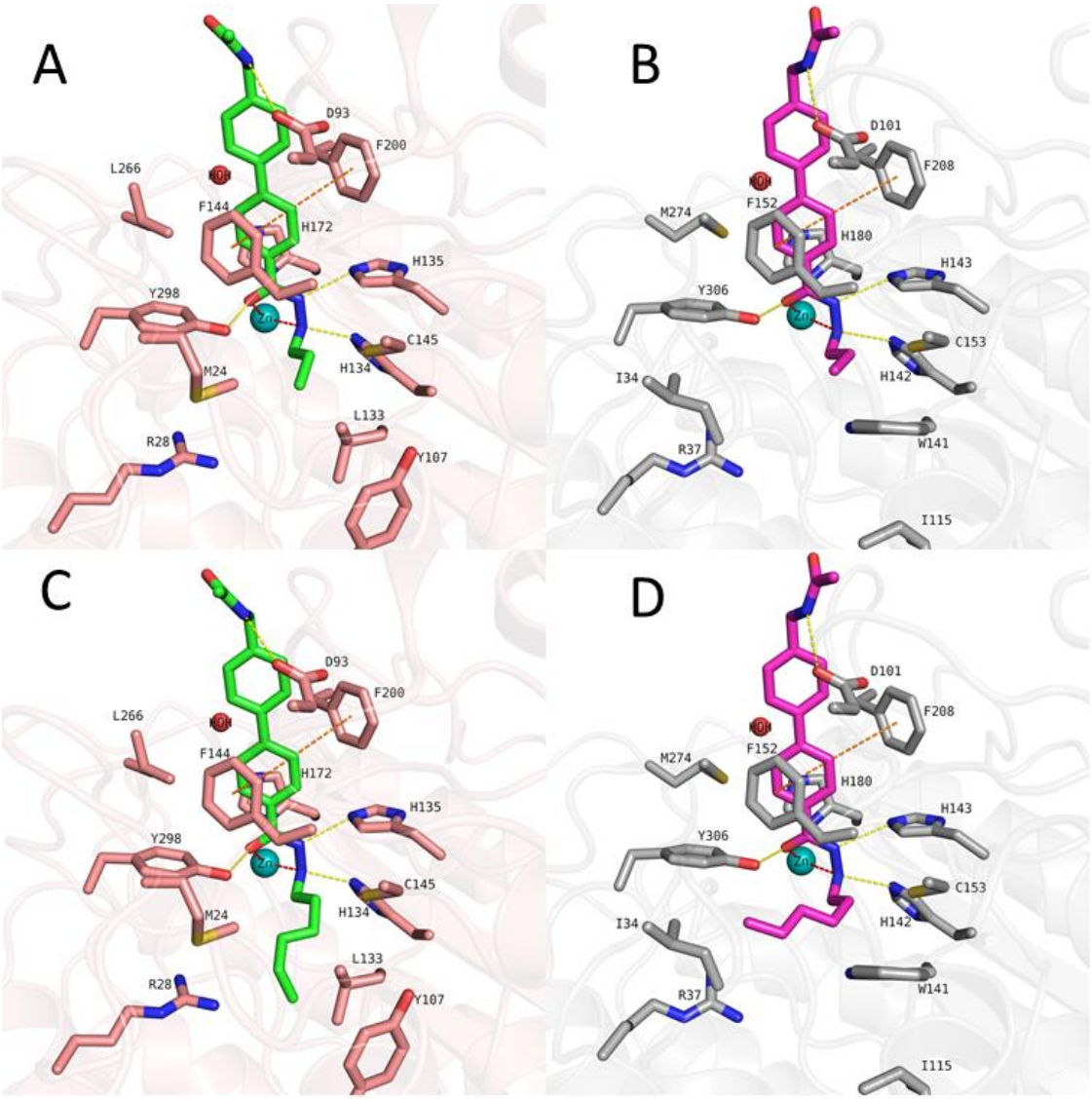

Figure 5. Docking poses of **7a** (A, green colored sticks) in HDAC3 (PDB ID: 4A69), **7a** (B, magenta colored sticks) in HDAC8 (PDB ID: 1T69), and **7d** (C, green colored sticks) in HDAC3 (PDB ID: 4A69), **7d** (D, magenta colored sticks) in HDAC8, (PDB ID 1T69). Hydrogen bonds (yellow dashed lines), aromatic interactions (orange dashed lines) and metal coordination (red dashed lines) between inhibitors and the protein are shown. Relevant residues are shown in stick representation with salmon carbon atoms in HDAC3 and grey carbon atoms in HDAC8. The zinc ion is shown as cyan colored sphere. The conserved water molecule is shown as red sphere.

In the second series of compounds bearing a substituted phenyl attached to the alkylhydrazide moieties, the meta-substituent on the phenyl linker group was found to target the side pocket of HDAC8. This represents a HDAC8-specific pocket which does not exist in HDAC1-3. In case of **7g**, the *m*-substituted benzylamino group

shows aromatic interactions with F152 and Y306 in the side pocket of HDAC8 which might be a further contribution factor for the selectivity over other HDACs. Meanwhile, the phenyl linker group is placed into the hydrophobic tunnel by interacting with F152 and F208 in HDAC8. The hydrazide zinc binding group chelates the zinc ion in a bidentate manner as well as showing hydrogen bond interactions with H142, H143 and Y306 in HDAC8. As observed for the previous series, the *n*-hexyl chain is placed into the foot-pocket of HDAC8, and makes hydrophobic interactions with I34 and W141 (Figure 6B). On the other hand, docking poses of **7g** in HDAC1-3 showed that the hydrazide moiety is not able to chelate the zinc in HDAC1-3 resulting in loss of HDAC1-3 activity (Figure 6A).

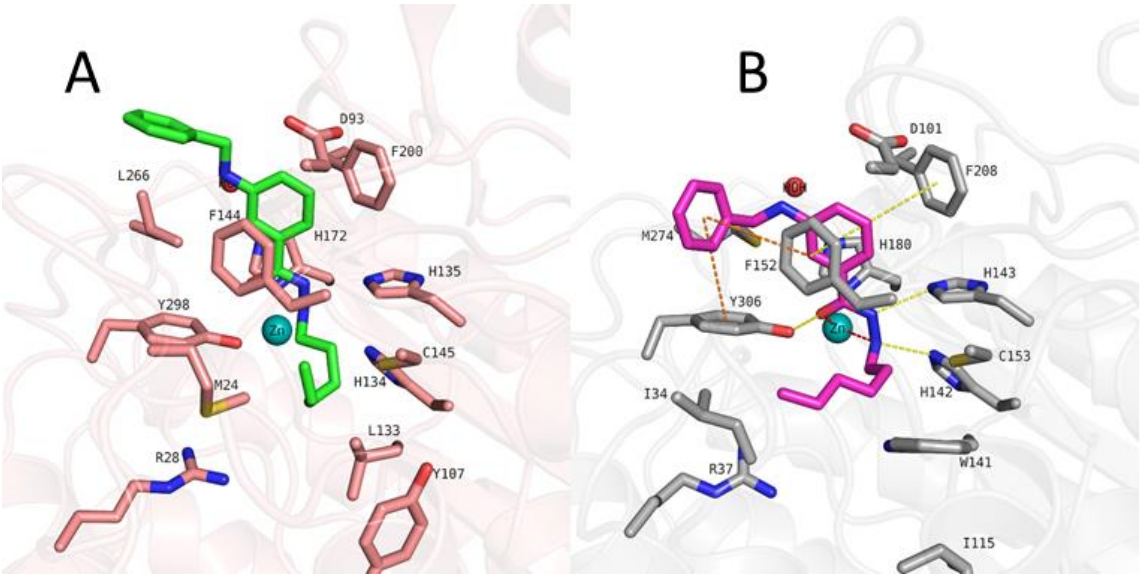

Figure 6. Docking poses of **7g** (A, green colored sticks) in HDAC3 (PDB ID: 4A69), **7g** (B, magenta colored sticks) in HDAC8 (PDB ID: 1T69). Hydrogen bonds (yellow dashed lines), aromatic interactions (orange dashed lines) and metal coordination (red dashed lines) between inhibitors and the protein are shown. Relevant residues are shown in stick representation with salmon carbon atoms in HDAC3 and grey carbon atoms in HDAC8. The zinc ion is shown as cyan colored sphere. The conserved water molecule is shown as red sphere.

The third series of designed compounds (**28a-m**), bearing different aromatic capping groups and different foot-pocket targeting alkyl chains, demonstrated similar

predicted binding modes as observed with their counterparts from the first series (exemplified by the docking poses of **28a** and **28l** in Figure 7). Again here, we could observe that the *n*-propyl chain is perfectly embedded into the foot-pocket region of HDAC3 resulting in selectivity for HDAC3 over other HDACs. The hydrazide group showed bidentate chelation as well as hydrogen bond interactions with H134, H135 and Y298 in HDAC3. Additionally, the pyrimidine ring is placed in the hydrophobic tunnel where it undergoes aromatic interactions with F144 and F200 in HDAC3. The benzylamino capping group showed additional aromatic interaction with F144 in HDAC3 (Figure 7A). The docking poses of **28a** in HDAC1-2 (not shown) and HDAC8 showed a similar binding pattern (Figure 7B). On the other hand, replacing the *n*-propyl chain by an *n*-hexyl chain resulted in an increased HDAC8 selectivity. As previously observed for similar compounds, the *n*-hexyl chain of **28l** was directed towards I34 and W141 in the foot-pocket of HDAC8 (Figure 7D), while in HDAC3 the hydrazide moiety could not be well accommodated in the foot-pocket and clashed with the M24, R28, L133 due to the steric hindrance resulting in a loss of HDAC3 activity (Figure 7C).

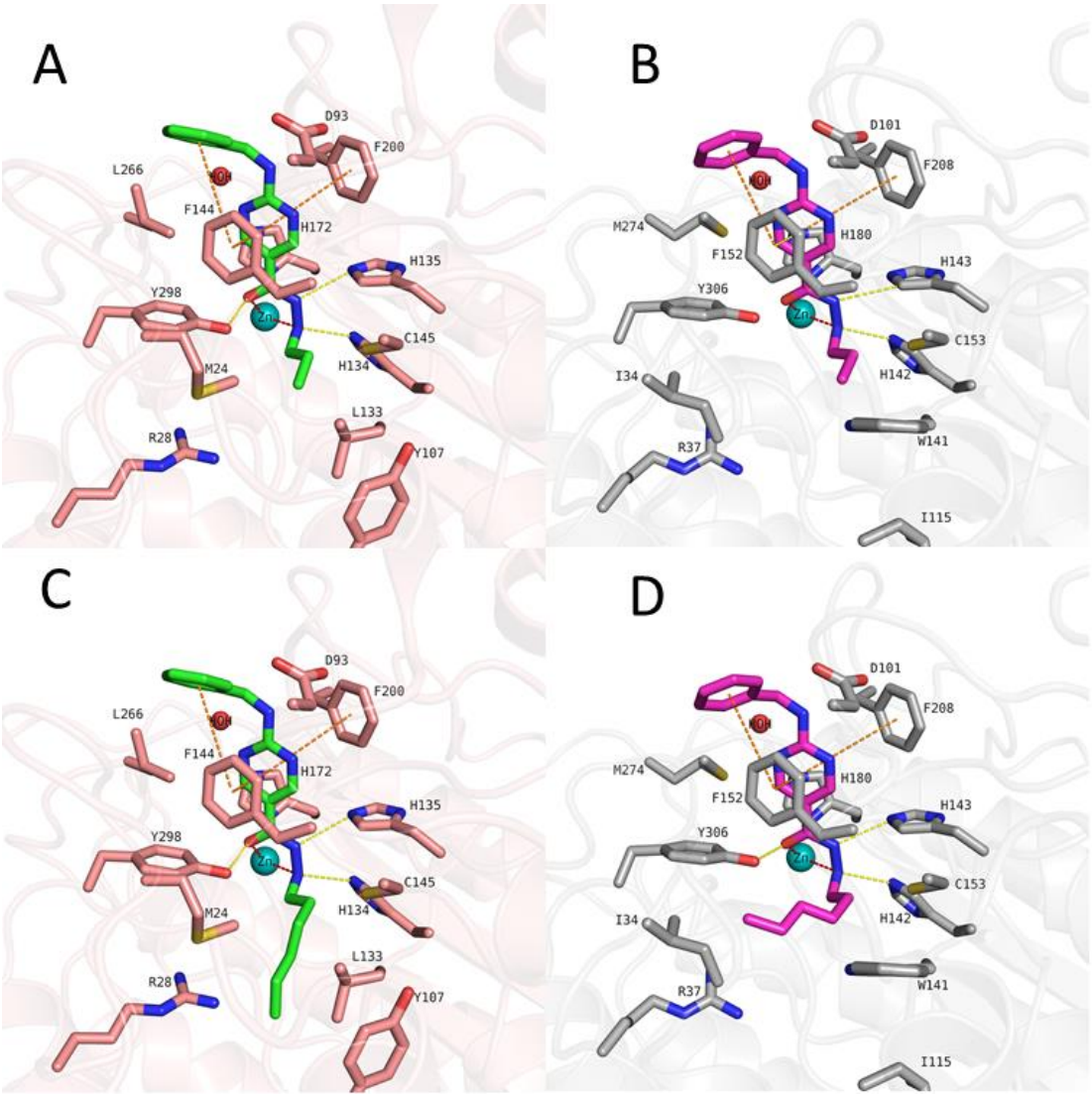

Figure 7. Docking poses of **28a** (A, green colored sticks) in HDAC3 (PDB ID: 4A69), **28a** (B, magenta colored sticks) in HDAC8 (PDB ID: 1T69), and **28l** (C, green colored sticks) in HDAC3 (PDB ID: 4A69), **28l** (D, magenta colored sticks) in HDAC8, (PDB ID 1T69). Hydrogen bonds (yellow dashed lines), aromatic interactions (orange dashed lines) and metal coordination (red dashed lines) between inhibitors and the protein are shown. Relevant residues are shown in stick representation with salmon carbon atoms in HDAC3 and grey carbon atoms in HDAC8. The zinc ion is shown as cyan colored sphere. The conserved water molecule is shown as red sphere.

The docking results of the last series of compounds **40b-d** having a n-hexyl chain are exemplified by the obtained docking poses of **40b** in Figure 8. The docking poses of **40b** revealed that the indole capping group is accommodated at the surface of the enzyme by establishing aromatic interactions with a phenylalanine residue (F200/208

in HDAC3/8, respectively), and the piperazine ring displays hydrogen bond interactions with a conserved aspartate (D101 in HDAC8). These additional interactions with phenylalanines (F200/208 in HDAC8, respectively) and aspartate (D101 in HDAC8) might be the reason behind the improved HDAC8 activity. Additionally, the pyrimidine linker group is located at the hydrophobic tunnel by showing aromatic interactions with F144/F200 and F200/F208 in HDAC3/8, respectively (Figure 8A/B). The *n*-hexyl chain is directed towards I34 and displays hydrophobic interaction with W141 resulting in selectivity for HDAC8 (Figure 8).

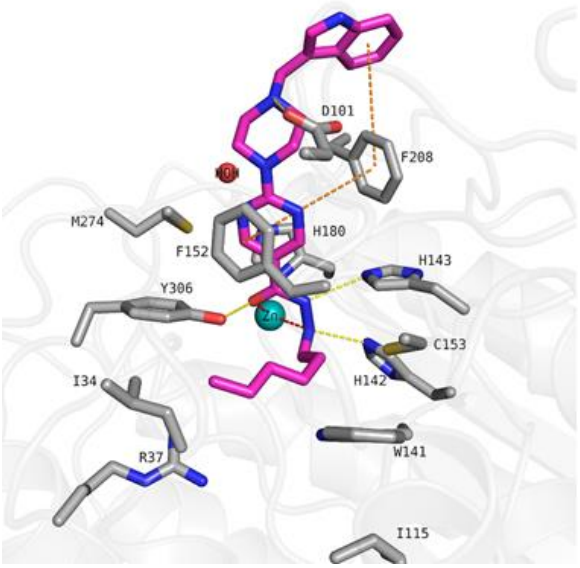

Figure 8. Docking poses of **40b** (magenta colored sticks) in HDAC8 (PDB ID: 1T69). Hydrogen bonds (yellow dashed lines), aromatic interactions (orange dashed lines) and metal coordination (red dashed lines) between inhibitors and the protein are shown. Relevant residues are shown in stick representation with salmon carbon atoms in HDAC3 and grey carbon atoms in HDAC8. The zinc ion is shown as cyan colored sphere. The conserved water molecule is shown as red sphere.

Stability testing for selected compounds

To test the chemical stability of the developed inhibitors under cellular assay conditions, we set up a non-enzymatic stability assay. Compounds were diluted in the cellular assay media (Dulbecco's Modified Eagle Medium (DMEM) (50%)/dimethyl

sulfoxide (10%)/acetonitrile (40%)) and were incubated at 37 °C for max. 72 h. The results of the non-enzymatic stability testing are presented in Table 7 and S2 in the Supplement. Under the applied conditions, **7a** and **7d** were found to be stable over 72 h at physiological pH 7.4 and 37 °C. **40a** showed significant degradation over the 72 h testing period.

Table 7. Stability of selected HDAC8 inhibitors in assay medium at 37°C.

inhibitor	0h - %	6h - %	12h - %	24h - %	48h - %	72h - %
7a	100.0	98.3	97.3	94.9	90.4	86.8
7d	100.0	102.7	104.2	105.2	104.0	103.1
40a	100.0	81.7	83.3	82.9	27.1	31.1

Cytotoxicity studies against healthy human cells

To test the potential toxicity of the active HDAC inhibitors, cytotoxicity tests were performed on human embryonic kidney-derived HEK293 cells. As shown in **Table 8**, the HDAC8 inhibitors with the exception of the indole derivatives **40b,c,e** showed weak to no cytotoxic effects (>40% cell viability) against HEK293 cells at a high concentration of 50 µM.

Table 8. HEK293 cytotoxicity of developed inhibitors.

ID	HEK293 cell viability at 50 µM	ID	HEK293 cell viability at 50 µM	ID	HEK293 cell viability at 50 µM
7a	83.9 ± 1.0	**28b**	88.9 ± 4.4	**28k**	90.1 ± 5.2
7b	80.1 ± 3.7	**28c**	80.5 ± 1.5	**28l**	88.4 ± 0.38

7c	90.8 ± 2.1	**28d**	78.9 ± 2.3	**28m**	79.4 ± 3.8
7d	121.3± 4.3	**28e**	80.7 ± 2.9	**40a**	47.0 ± 4.4
7e	81.2 ± 4.6	**28f**	83.2 ± 3.3	**40b**	2.18 ± 0.2
7f	113.3 ± 5.5	**28g**	78.2 ± 5.7	**40c**	1.6 ± 0.9
7g	71.2 ± 3.9	**28h**	93.6 ± 3.7	**40d**	47.1 ± 7.4
7h	41.7 ± 7.7	**28i**	93.1 ± 6.5	**40e**	31.8 ± 3.0
28a	80.9 ± 2.4	**28j**	65.7 ± 3.9	**Dauno-rubicin**	1.2 ± 0.2 μM

Selective class I HDAC inhibitory activity in Jurkat T lymphocytes

To further investigate target engagement and selectivity of these novel hydrazide-based HDAC8 inhibitors, we selected a subset of active inhibitors from the different series and performed western blot experiments with 10 μM representative compounds and PCI-34051 (25 μM) as control in HDAC8-expressing Jurkat $CD4^+$ T lymphocyte cell line[28] (Figure 9). Treatment of Jurkat cells with most of the selected hydrazide-based HDAC inhibitors for 6 h could increase the acetylation levels of H3K27 and H3K9 (class I HDAC substrates)[16,46-48] as compared to the reference inhibitor PCI-34051 (Figure 9). Notably, strong H3K27 acetylation was observed for **7d, 28i, 28j, 28k, 28m, 40a, 40b, 40c**, and **40e**, while no hyperacetylation of the HDAC6 substrate tubulin was noted.

.

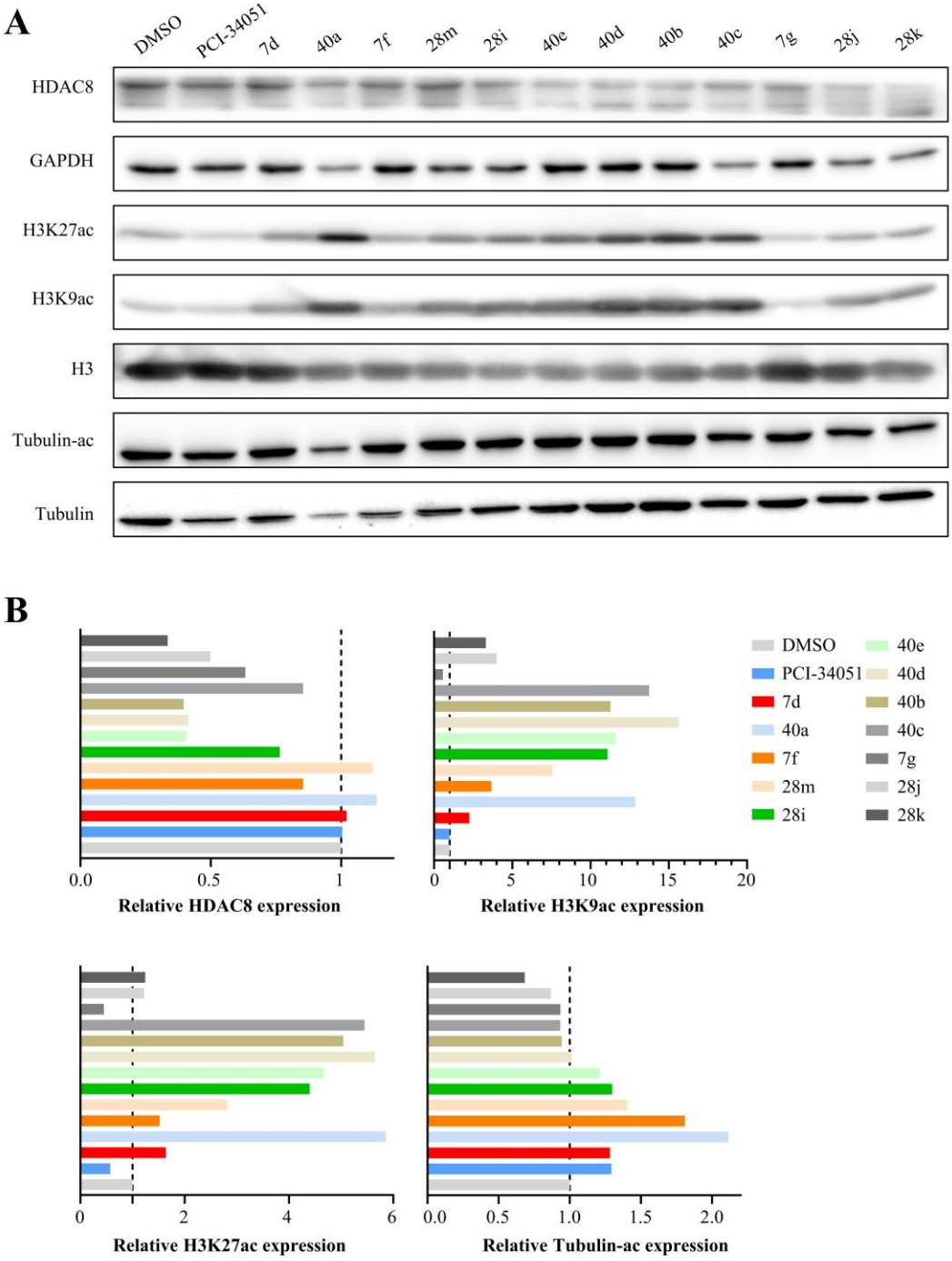

Figure 9. Western blot analysis of H3K9, H3K27 and α-tubulin acetylation in 6.25×10^5 Jurkat T lymphocytes treated with the developed hydrazide-based HDAC8 inhibitors at 10 μM and reference inhibitor PCI-34051 at 25 μM for 6 h. GAPDH, histone H3 and tubulin were used as a loading control.

Gene expression analysis of 7d in Jurkat T lymphocytes

Our previous study demonstrated that selective HDAC8 inhibition can significantly enhance the efficacy and durability of HCC therapy by immune-checkpoint blockade, which was accompanied by an induction of memory T cell response.[16] From the *in vitro*, stability and target engagement results, **7d** showed the most promising effects and was selected as lead compound for further gene expression characterization.

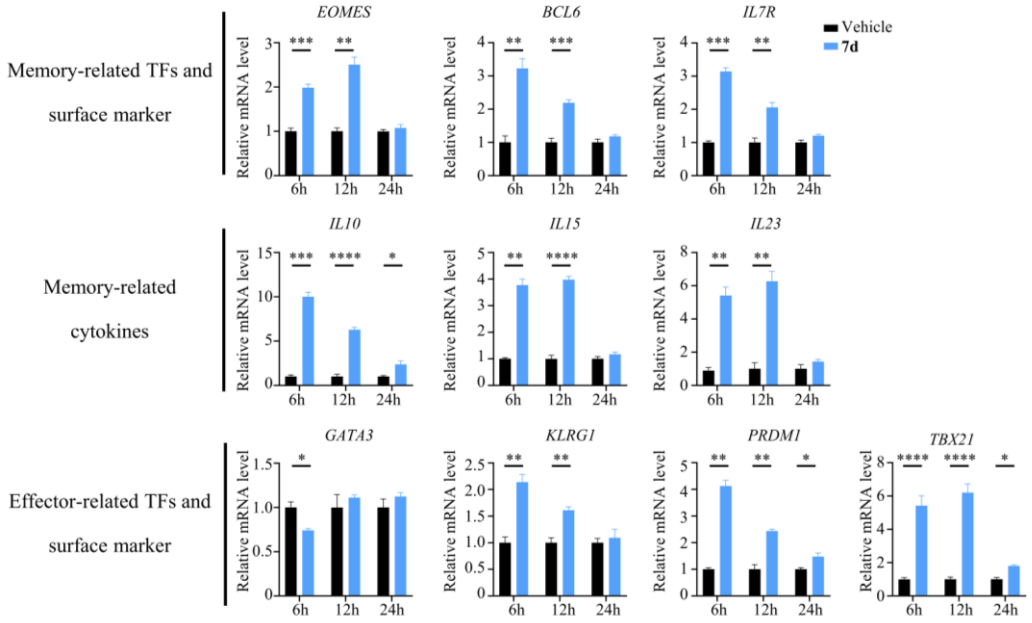

Figure 10. RT-qPCR analysis of T cell memory and effector genes in 6.25×10^5 Jurkat lymphocytes treated with **7d** at 10 μM for 6 h, 12 h and 24 h. *GAPDH* was used for normalization. T-test was used for statistical analysis. * $p<0.05$; ** $p<0.01$; *** $p<0.005$; **** $p<0.001$.

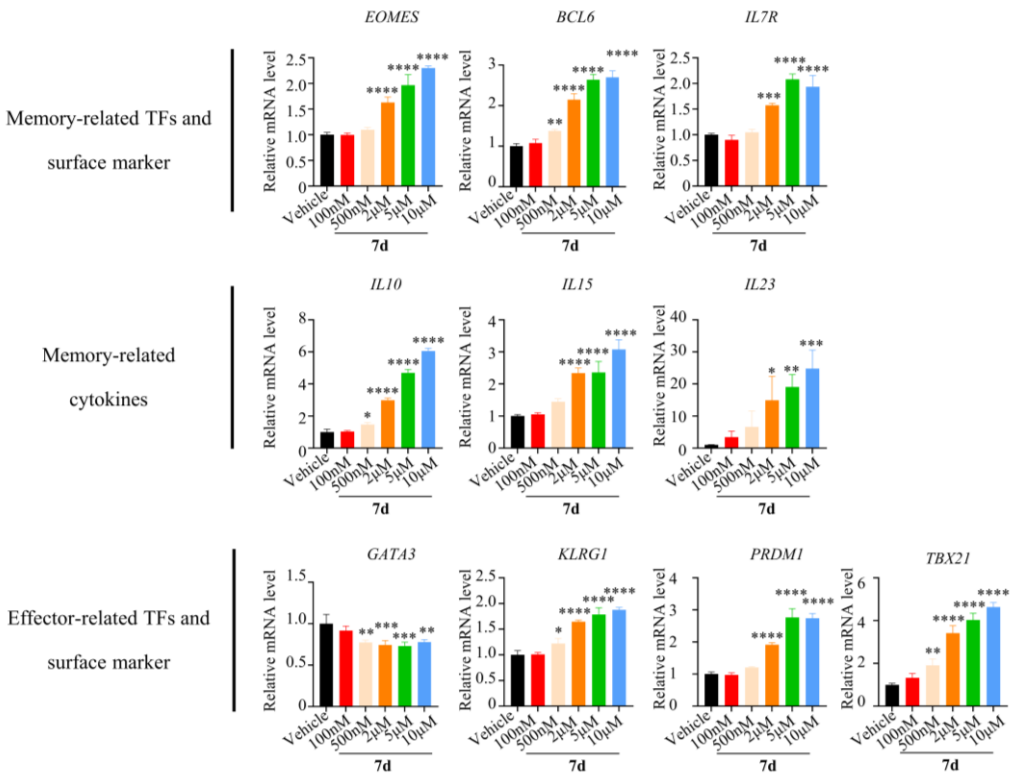

Figure 11. RT-qPCR analysis of T cell memory and effector genes in 6.25 × 10^5 Jurkat lymphocytes treated with **7d** at indicated concentrations for 6 h. *GAPDH* was used for normalization. One-way ANOVA was used for statistical analysis. * p<0.05; ** p<0.01; *** p<0.005; **** p<0.001.

Using RT-qPCR, we found that 10 μM **7d** can remarkably up-regulate memory-related transcription factors (TFs: *Bcl6, Eomes*), surface marker (*Il7r*) and cytokines (*Il10*, *Il15*, *Il23*) as well as effector-related master regulators (*Prdm1*, *Tbx21*) and surface marker (*Klrg*) in Jurkat T lymphocytes treated for 6 h and 12 h (Figure 10). Consistent results were observed in Jurkat T lymphocytes treated by 25 μM PCI-34051 (data not shown). Moreover, **7d** can dose-dependently up-regulate these T cell memory- and effector-related genes upon 6 h treatment (Figure 11).

Gene expression analysis of 7d in $CD4^+$ T lymphocytes

To verify the gene modulatory effects of **7d** in T lymphocytes, we isolated $CD4^+$ T lymphocytes from the spleen of immunocompetent C57BL/6 mice, followed by *ex vivo* culture with 5, 10 μM **7d** or DMSO vehicle control for 6 h (Figure 12A). Consistent with the data in Jurkat T lymphocytes, **7d** treatment of HDAC8-expressing $CD4^+$ T lymphocytes increased the H3K27 acetylation level (Figure 12B). As a SMC3 deacetylase[49], we found that HDAC8 inhibition by **7d** also markedly increased SMC3 acetylation level (Figure 12B). Moreover, **7d** could significantly up-regulate most of the detected T cell memory- and effector-related genes in $CD4^+$ T lymphocytes (Figure 12C).

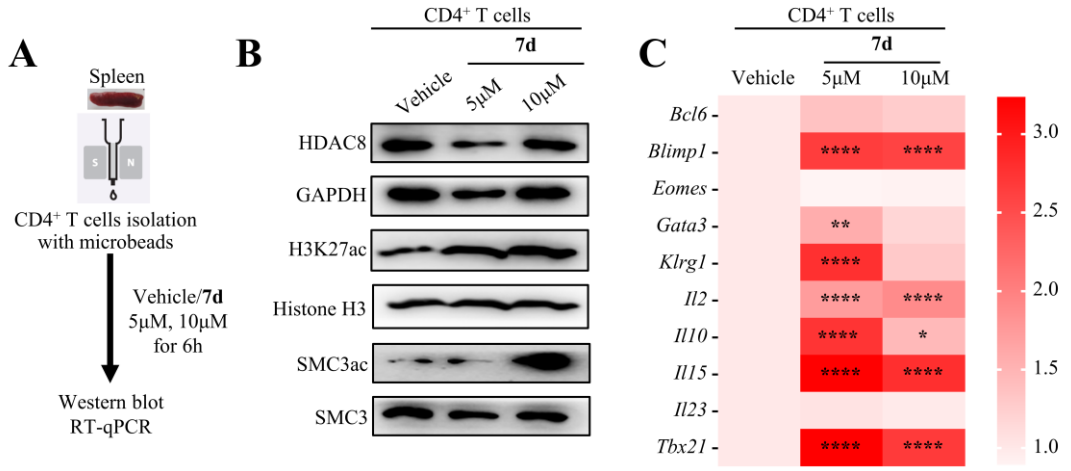

Figure 12. Gene expression analyses of mouse primary $CD4^+$ T cells treated with **7d**. (A) A schematic diagram of $CD4^+$ T cell isolation from spleen and treatment. (B) Western blot and (C) RT-qPCR analyses of HDAC8 and its substrates SMC3 and H3K27 as well as T cell memory and effector genes in 2×10^6 $CD4^+$ T cells treated with **7d** at 5 and 10 μM or DMSO control for 6 h. *GAPDH* was used for normalization. One-way ANOVA was used for statistical analysis. * $p<0.05$; ** $p<0.01$; **** $p<0.001$.

Immune-modulatory effect of 7d *in vivo*

The results of gene expression analysis in T lymphocytes suggest that **7d** may exert immune-modulatory effect. We further studied this by intraperitoneal (i.p.)

administration of 5, 10 mg/kg **7d** or vehicle control 5 days per week for 2 weeks in C57BL/6 mice, which is a common animal model used for immune-related diseases[16] (Figure 13A).

Using flow cytometry, we found that 10 mg/kg **7d** significantly increased the proportions of $CD3^+$ and $CD8^+$ but not $CD4^+$ T cells in the spleen of treated mice compared to vehicle control (Figure 13B). Interestingly, RT-qPCR analysis of some key T cell memory and effector genes (*Bcl6*, *Klrg1*, *Il2*, *Il15*, *Tbx21*) showed that 10 mg/kg **7d** significantly induced the expression of *Il2* in the sorted $CD4^+$ but not $CD8^+$ T cells (Figure 13C), supporting the immune-modulatory function of **7d** *in vivo*. Furthermore, treatment with **7d** was in general well-tolerated, as we did not observe any body and organ weight change (Figure 13D and 13E) or abnormalities in the heart, intestine, kidney, liver, lung, spleen and stomach (Figure 13F).

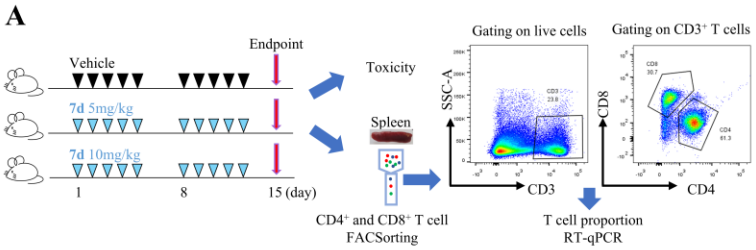
A
Vehicle
7d 5mg/kg
7d 10mg/kg
Endpoint
1
8
15 (day)
Toxicity
Spleen
CD4⁺ and CD8⁺ T cell FACSorting
Gating on live cells
SSC-A
CD3
Gating on CD3⁺ T cells
CD8
CD4
T cell proportion RT-qPCR

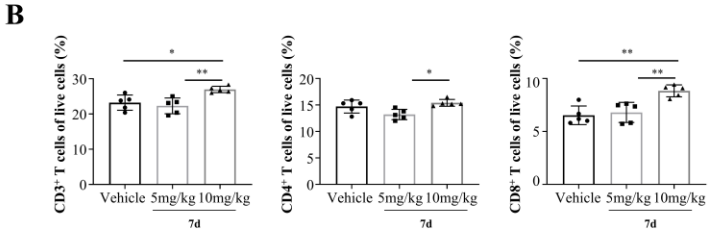
B
CD3⁺ T cells of live cells (%)
CD4⁺ T cells of live cells (%)
CD8⁺ T cells of live cells (%)
Vehicle
5mg/kg
10mg/kg
7d

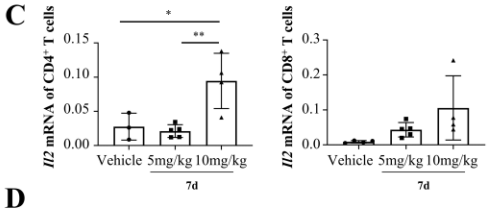
C
Il2 mRNA of CD4⁺ T cells
Il2 mRNA of CD8⁺ T cells
Vehicle
5mg/kg
10mg/kg
7d

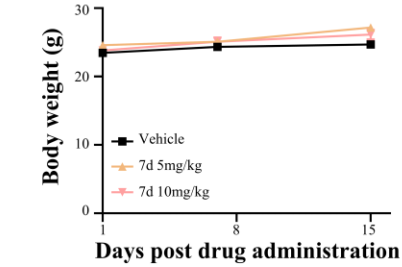
D
Body weight (g)
Vehicle
7d 5mg/kg
7d 10mg/kg
Days post drug administration

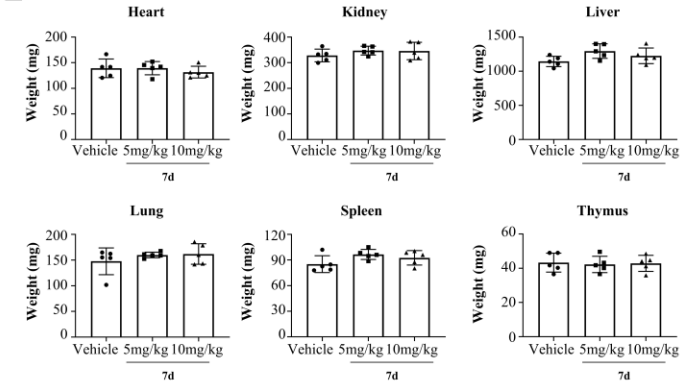
E
Heart
Kidney
Liver
Lung
Spleen
Thymus
Weight (mg)
Vehicle
5mg/kg
10mg/kg
7d

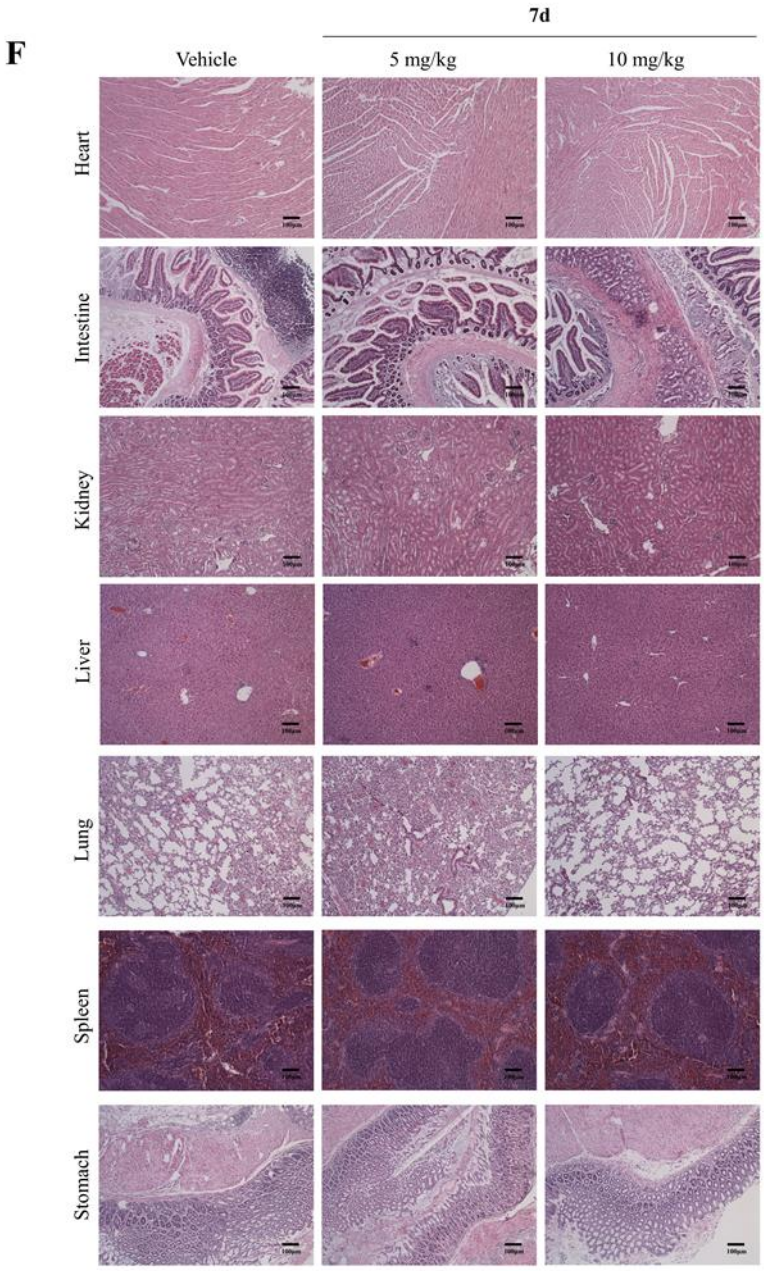

Figure 13. Immune and toxicity analyses of C57BL/6 mice treated with **7d**. (A) A schematic diagram of administration of **7d** (5, 10 mg/kg i.p.) or vehicle control (30% PEG400 + 0.5% Tween 80 + 5% propylene glycol), flow cytometry and RT-qPCR analyses. (B) Proportions of $CD3^+$, $CD4^+$ and $CD8^+$ T cells in the spleen of mice treated with **7d** or vehicle control (n=5). (C) RT-qPCR analysis of *Il2* in sorted $CD4^+$ and $CD8^+$ T cells treated with **7d** or vehicle control (n=5). *GAPDH* was used for normalization. One-way ANOVA was used for statistical analysis. * $p<0.05$; ** $p<0.01$. (D) Body weight following drug administration, (E) organ weight and (F) histological analysis by hematoxylin and eosin staining (100x magnification) at 15-day post-treatment of mice treated with **7d** or vehicle control (n=5).

Conclusion

In this study, we have systematically optimized the structure of alkylhydrazides as class I HDAC inhibitors by the alteration of the foot-pocket targeting group (length of *N*-alkyl side chain attached to the hydrazide unit), linker and capping group. Interestingly the use of *n*-hexyl groups attached to the hydrazide moiety resulted in selective HDAC8 inhibitors *in vitro*. Docking studies suggest that the *n*-hexyl side chain of alkylated hydrazides is well accommodated to the size and form of the HDAC8 foot-pocket, while the *n*-propyl side chain is favourable for the HDAC3 foot-pocket. Enzyme kinetic study for HDAC8 indicates the representative compounds **7d** and **40a** as substrate competitive and reversible inhibitors which is also supported by the docking results where the alkylhydrazide is showing a bidentate chelation of the zinc ion. The promising inhibitor **7d** was found to be stable in a non-enzymatic stability assay and showed a safe profile into a cytotoxicity assay using HEK293 cells. HDAC8 target engagement was shown by western blotting the hyperacetylation of SMC3 and H3K27.

We have recently reported HDAC8 over-expression in driving HCC malignancy[15] and immunotherapy resistance through potent exclusion of T cells from the tumor microenvironment.[16] The function of tumoral HDAC8 is unique as it aberrantly regulates chemokine enhancers through specific deacetylation of H3K27, representing a new chromatin mechanism of tumor immune evasion.[16] Moreover, selective inhibition of HDAC8 by PCI-34051 synergized with immune-checkpoint blockade antibody to potentiate robust T cell-mediated cytotoxicity and durable survival benefit, which was accompanied by strong memory T cell induction.[16] In this study, we

therefore tested whether the new alkylated hydrazides exhibit a T cell modulatory effect. Using both Jurkat and primary T cell models, we demonstrated that **7d** can selectively up-regulate acetylation levels of two HDAC8 substrates (H3K27 and SMC3) and gene expressions of several key memory- and effector-related TFs and cytokines in $CD4^+$ T lymphocytes.

One notable biological effect of **7d** is the induction of $CD8^+$ T lymphocytes in the spleen. This immune enhancement may be mediated via IL-2 up-regulation in $CD4^+$ T lymphocytes, which is an important cytokine for $CD8^+$ T cell proliferation and survival[50]. Similar to PCI-34051 (25 mg/kg), administration of **7d** (10 mg/kg) *in vivo* was found to be safe without body weight loss or internal organs' abnormalities. In summary, this study not only identifies the alyklhydrazide as chemotype for class I HDAC selective inhibitors to overcome limitations of current hydroxamate based inhibitors, but also provides interesting T cell modulatory effects for further therapeutic investigation.

Materials and methods

1. General

All materials and reagents were purchased from Sigma-Aldrich Co. Ltd. and abcr GmbH. All solvents were analytically pure and were dried before use. Thin layer chromatography was carried out on aluminium sheets coated with silica gel 60 F254 (Merck, Darmstadt, Germany). For medium pressure chromatography (MPLC) silica gel Biotage® SNAP ultra-HP-sphere 25 µm containing columns were used. For column chromatography, silica gel 60 (0.015-0.04 mm) from the manufacturer Merck KgaA was used as a stationary phase.

Dichloromethane: methanol; *n*-hexane: ethyl acetate were the elution systems used for medium pressure chromatography and column chromatography. Triethylamine was added in a concentration of 0.1 % to dichloromethane or ethyl acetate, according to the solvent system used, in purification of compounds having free amine.

In the preparative high-pressure chromatography used for cleaning of several final compounds, LiChrosorb® RP-18 (7 µm) 250-25 Merck column was used. The applied mobile phase was a gradient with increasing polarity composed of acetonitrile/water.

Final compounds´ purity was determined using high-pressure chromatography (HPLC). Purity was measured by UV absorbance at 254 nm. Two analytical methods were used while determining the purity. In the first method (M1), the components of the HPLC were an XTerra RP18 column (3.5 mm, 3.9 mm x 100 mm) from the manufacturer Waters (Milford, MA, USA) and two LC-10AD pumps, a SPD-M10A VP PDA detector, and a SIL-HT autosampler, all from the manufacturer Shimadzu (Kyoto, Japan). In the second method (M2), only the column was changed to LiChrosorb® RP-18 (5 µm) 100-4.6 Merck column.

Microwave reactions were performed by heating to the corresponding temperature within 5 min through a microwave reactor (Monowave 450 from the manufacturer Anton Paar GmbH).

Mass spectrometry analyses were performed with a Finnigan MAT710C (Thermo Separation Products, San Jose, CA, USA) for the APCI spectra and with an LTQ (linear ion trap) Orbitrap XL hybrid mass spectrometer (Thermo Fisher Scientific, Bremen, Germany) for the HRMS-ESI (high resolution mass spectrometry) spectra.

For the HRMS analyses, the signal for the isotopes with the highest prevalence was given and calculated (35Cl, 79Br).

^{1}H NMR and ^{13}C NMR spectra were taken on a Varian Inova 500/Varian Gemini 2000 using deuterated chloroform or deuterated dimethylsulfoxide as solvent. Chemical shifts are referenced to the residual solvent signals.

2. General synthetic methods

Method I, Hydrazide mono-alkylation

A. To a stirred mixture of hydrazide (1.0 mmol), anhydrous Na_2SO_4 (0.5 g) and p-toluenesulfonic acid (pTSA) (0.05 mmol) in MeOH (5 mL) was added dropwise corresponding aldehyde (1.05 mmol). The mixture was stirred at room temperature for 2h followed by addition of $NaBH(AcO)_3$ (2.0 mmol) to the reaction. The resulting mixture was stirred for an additional 1h. Then, saturated Na_2CO_3 solution was added to the mixture until pH ≈ 10. The mixture was extracted with DCM and water three times. The collected organic layers were washed with brine, dried over anhydrous Na_2SO_4 and concentrated. The residue was purified by column chromatography (EtOAc : heptane = 1 : 10 to 1 : 3 gradually) to give pure intermediates **2a-d** as white solid. The yield was between 47-90 %.

B. $NaBH(AcO)_3$ (3.0 mmol) was added to a stirred mixture of aldehyde (1.1 mmol) and hydrazide (1.0 mmol) in DCM (3 mL). The resulting mixture was stirred at room temperature overnight. Saturated Na_2CO_3 solution was then added dropwise to the reaction until no bubbles appeared. The reaction was washed with water two times. The collected organic layer was dried over anhydrous Na_2SO_4 and concentrated. The

residue was purified by column chromatography (EtOAc: heptane = 1 : 15, 1 : 10 and then DCM : MeOH = 30 : 1 gradually) to give pure intermediates or final compounds.

C. To a stirred mixture of hydrazide (1.0 mmol), pTSA (0.05 mmol) and anhydrous Na_2SO_4 (0.6 g) in MeOH (4 mL) was added aldehyde (1.05 mmol). An additional DCM (2.0 mL) was added to the reaction if the reaction was not easy to be stirred. The resulting mixture was stirred for 2h at room temperature. $NaBH_4$ (4.00 mmol) was then added to the reaction over three portions and the stirring was continued for 1h. Saturated Na_2CO_3 solution was added to the mixture until no bubbles appeared. The reaction was extracted with water and DCM two times. The combined organic layers were dried over anhydrous Na_2SO_4 and concentrated. The residue was purified by column chromatography (DCM : MeOH = 1 : 0, 40 : 1, 30 : 1 gradually) to give pure intermediates or final compounds.

Method II, Suzuky coupling

A stirred mixture of boronic acid **(11 or 10)** (1.4 mmol), iodobenzohydrazide (**3a-d**) (1.27 mmol), $Pd(PPh_3)_4$ (0.05 mmol) and K_2CO_3 (3.18 mmol) in a solution of toluene (18 mL), MeOH (2 mL) and H_2O (2 mL) was kept under argon atmosphere and heated to 90 ^oC for 7h. The reaction was directly concentrated and the residue was purified by column chromatography (EtOAc : heptane = 1 : 4 to 1 : 2 gradually) to give **4** and **8b-d** as white solid.

Method III, Protective goup protection and deprotection for amine

A. Boc-protection

To a stirred mixture of the corresponding amine (1.0 mmol) and TEA (2.5 mmol) in THF or DCM (6 mL) was added $(Boc)_2O$ (1.1 mmol). The reaction was stirred at

room temperature overnight. The reaction was concentrated and the residue was purified by column chromatography (EtOAc : heptane = 1 : 15, 1 : 10 to 1 : 5) to give pure Boc-protected intermediates.

B. Boc-deprotection

A Boc-protected intermediate was added in a solution of HCl/dioxane (4M) and DCM (2 : 5). The resulting mixture was stirred at room temparature for 3h. Then, saturated Na_2CO_3 solution was added to the mixture until no bubbles appeared. The mixture was extracted with DCM and brine three times. The combined organic layers were dried over anhydrous Na_2SO_4 and concentrated. The residue was purified by column chromatography (EtOAc : heptane = 1 : 5 and then DCM : MeOH = 1 : 0 to 25 : 1) to give Boc-deprotected intermediate or final compound. For intermediate **24**, the reaction was directly evaporated to give **24** as light yellow solid. For **33**, the precipitate was filtered and dried to give compound **33** as white solid.

C. Cbz-protection

Benzyl chloroformate (14.5 mmol) was added dropwise to a stirred mixture of 4-(aminomethyl)benzoic acid (**12**) (13.2 mmol) and Na_2CO_3 (53 mmol) in water (100 mL) under ice bath. The resulting mixture was stirred for an additional 1.5h and precipitate appeared. Then, a HCl (1N) solution was added dropwise to the mixture until pH ≈ 3. The precipitate was filtered. The white residue was dried to yield intermediate 4-((((benzyloxy)carbonyl)amino)methyl)benzoic acid (**13**) as white solid.

D. Cbz-deprotection

Pd/C (10 %) (140 mg) was added to a mixture of Cbz-protected intermediate (1.85 mmol) in MeOH (15 mL) at room temperature and followed by $NaBH_4$ (9.25 mmol)

by three portions. The reaction was charged with a balloon each $NaBH_4$ addition and stirred overnight. The mixture was filtered. The collected filtrate was extracted with EtOAc and brine three times. The combined organic layers were washed with brine three times, dried over anhydrous Na_2SO_4 and concentrated to give Cbz-deprotected product that was used without further purification

E. Benzyl-protection

Benzylchloride (1.74 mmol) was added to a mixture of tert-butyl piperazine-1-carboxylate (**31**) (10.74 mmol) and K_2CO_3 (62.3 mmol) in EtOH (20 mL). The resulting mixture was refluxed overnight. The mixture was filtered. The filtrate was concentrated and the resulting residue was purified by column chromatography to give intermediate **32**.

F. Benzyl-deprotection

A stirred mixture of benzyl-protected intermediate (1.0 mmol), Pd/C (10 %) (40 mg) and ammonium formate (4.0 mmol) in MeOH (5 mL) was heated to about 60 ^oC for 4h. The reaction was filtered. The resulting filtrate was evaporated and the residue was extracted with EtOAc and brine three times. The combined organic layers were dried over anhydrous Na_2SO_4 and concentrated to give benzyl-deprotected product.

Method IV, Amide bond formation

A. Between ester and hydrazine

1. A stirred mixture of hydrazine monohydrate (30.0 mmol) and ester (1.0 mmol) in EtOH (3 ml) was refluxed for 3h until the reaction become clear. The reaction was

cooled to room temperature. The precipitate was filtered. The white residue was washed with cold water and dried to give corresponding hydrazide as white solid.

2. A mixture of ester (1.0 mmol) and hydrazine monohydrate (10.0 mmol) in EtOH (1 ml) was heated to 110 ^{o}C in a microwave reactor for 1h. The reaction was then evaporated. The resulting residue was washed with cold water and dried to give the corresponding hydrazide as white solid.

B. Between carboxylic acid and hydrazine

CDI (Carbonyldiimidazole) (11 mmol) was added to a stirred mixture of carboxylic acid (10.51 mmol) in THF (40 mL). The reaction was stirred for an additional 30 min at room temperature. Hydrazine monohydrate (105 mmol) was then added dropwise to the reaction and the resulting mixture was stirred at room temperature overnight. The reaction was evaporated. Water (50 mL) was added to the residue and precipitate appeared. The precipitate was filtered and washed with cold water two times. The white solid was dried to give intermediate **14** as white solid

C. Between acetyl chloride and amine

1. Acetylchloride (10.7 mmol) was added dropwise to a stirred mixture of (4-(aminomethyl)phenyl)boronic acid hydrochloride (**9**) (5.33 mmol) and DIPEA (18.7 mmol) in DCM (10 mL) at room temperature. The reaction was stirred for an additional 1h at room temperature. Then, the reaction was concentrated and purified by column chromatography (EtOAc : heptane and then DCM : MeOH gradually) to give compound **10** as white solid (yield: 59 %).

2. Acetyl chloride (1.5 mmol) was added to a stirred mixture of amine (1.0 mmol) and DIPEA (3.0 mmol) in DCM (2.5 mL) at room temperature. The resulting reaction was

stirred for 30 min. The reaction was concentrated and the residue was purified by column chromatography (DCM : MeOH = 1 : 0, 30 : 1 to 20 gradually) to give corresponding product.

Method V, Bromide and chloride substitution

A. A mixture of aniline (**19a** or **19b**) (1.1 mmol), benzyl chloride (1.0 mmol) and K_2CO_3 (2.5 mmol) in DMF (2 mL) was heated to 100 ^oC in a microwave reactor for 2h. The reaction was extracted with water and EtOAc twice. The combined organic layers were washed with brine, dried over anhydrous Na_2SO_4 and concentrated. The resulting residue was purified by MPLC to give **20a** or **20b** as colorless oil in around 22 % yield.

B. A mixture of ethyl 2-chloropyrimidine-5-carboxylate (**25**) (1.0 mmol), amine (1.0 mmol) and DIPEA (2.5 mmol) (DIPEA 3.5 mmol for amine HCl salt) in DCM (10 mL) was stirred at room temperature for 30 min. The reaction was extracted with DCM and water three times. The combined organic layers were dried over anhydrous Na_2SO_4 and concentrated. The residue was purified by column chromatography (EtOAc : heptane = 1 : 5 and then DCM : MeOH = 1 : 40) to give intermediate **26** as white solid. Another work-up procedure of **26**: Upon consumption, the reaction was washed with a HCl (10 %) solution three times and followed by brine. The collected organic layer was dried over anhydrous Na_2SO_4 and concentrated to give **26** that was used without further purification.

C. A stirred mixture of amine (**38b**) (1.0 mmol), 3-(2-bromoethyl)-indole or 3-(2-bromoethyl)-1-methyl-indole (1.2 mmol) and K_2CO_3 (2.5 mmol) in DMF (4 mL) was heated to about 80 ^oC overnight. The mixture was extracted with EtOAc and water two times. The combined organic layers were washed with brine two times, dried over

anhydrous Na_2SO_4 and concentrated. The resulting residue was purified by column chromatography (EtOAc : heptane = 1 : 1 and then DCM : MeOH = 30 : 1, 25 : 1) to give **39d** and **39e** respectively**.**

Method VI, Indole methylation

NaH (60 %) (8.9 mmol) was added to a stirred solution of 3-(2-bromoethyl)-indole (**29**) (1.78 mmol) in THF (5 mL). The mixture was stirred for several minutes followed by addition of CH_3I (17.8 mmol). The resulting reaction was stirred at room temperature overnight. Then, a solution of HCl (10 %) was added dropwise to the mixture until no bubbles appeared. The reaction was extracted with EtOAc and brine three times. The combined organic layers were washed with brine, dried over anhydrous Na_2SO_4, and concentrated. The residue was purified by column chromatography (EtOAc : heptane = 1 : 15) to give **30** as light yellow oil (0.25 g, yield: 59%)

Method VII, Reductive amination

A mixture of amine (**38a** or **38b**) (1.0 mmol), indole-3-carbaldehyde or 1-methyl-indole-3-carbaldehyde (1.0 mmol) and $NaHB(AcO)_3$ (2.0 mmol) in DCM (4 mL) was stirred at room temperature overnight. The reaction was then concentrated. The resulting residue was purified by column chromatography (EtOAc : heptane = 1 : 1 and then DCM : MeOH = 30 : 1, 25 : 1) to respectively give **39a-c**.

3. Computational Studies

The available protein structures were downloaded from the Protein Data bank (PDB) (PDB ID: 4BKX, 4LXZ, 4A69, 5EDU, 1T69, for HDAC1, 2, 3, 6, 8, respectively).

The HDAC1 (PDB ID: 4BKX) in apo-form and HDAC3 (PDB ID: 4A69) in apo-form were minimized with the SAHA compound of HDAC2 (PDB ID: 4LXZ). Protein structures were prepared by adding hydrogen atoms and missing side chains in the Protein Preparation Wizard module in Schrödinger Suite (Schrödinger Release 2020-2: LigPrep, Schrödinger, LLC: NewYork, NY, 2020). All water molecules (except one conserved water) and all ions (except zinc) were removed from the X-ray structures. The protonation states and tautomeric forms of the amino acids were optimized using PROPKA tool at pH 7.0. The optimized protein structures were minimized using OPLS3e force-field. Ligands were prepared using OPLS3e force-field in LigPrep module of Schrödinger Suite. The output of the LigPrep was applied to the Confgen tool in Schrödinger Suite by applying 64 conformers per each ligand and minimizing the conformers. Molecular docking studies were performed using the standard precision (SP) mode with flexible ligand samplingand enhance planarity of the conjugated pi groups in the Glide program of Schrödinger Suite. The grid box was generated with 10*10*10 Å size using the Receptor Grid Generation module in Schödinger. The docking protocols were validated by re-docking studies. The RMSD values of the re-docking studies corresponding to the binding mode in HDAC1/2/3/6/8 are observed less than 2Å for each isoform. Docking poses were visualized in MOE2019.01 program (Molecular Operating Environment (MOE), version 2019.01; Chemical Computing Group Inc., Montreal, Canada).

All the herein described compounds were filtered for pan-assay interference compounds (PAINS). For this purpose, PAINS1, PAINS2 and PAINS3 filters, as implemented in Schrödinger's Canvas program, were employed. None of the compounds was flagged as PAINS.

4. Non-enzymatic stability data

To test the non-enzymatic stability of the developed compounds they were diluted in the assay media of Dulbecco's Modified Eagle Medium (DMEM) (50 %)/dimethylsulfoxid (10 %)/acetonitrile (40 %) mixture at pH7.4, and incubated at 37 °C for max. 72 h. Quantity of the compounds was measured after 6, 12, 24, 48 and 72 hours by HPLC using XTerra RP18 column (3.5 mm, 3.9 mm x 100 mm) from the manufacturer Waters (Milford, MA, USA) and two LC-10AD pumps, a SPD-M10A VP PDA detector, and a SIL-HT autosampler, all from the manufacturer Shimadzu (Kyoto, Japan).

5. Enzymatic inhibitory activity and inhibition type confirmation

Recombinant human HDAC1, HDAC2 and HDAC3/NCOR1 were purchased from ENZO Life Science AG (Lausen, CH). Recombinant human HDAC8 and recombinant human HDAC11 was expressed and purified as described before[44, 51]. The HDAC1-3 *in vitro* testing was done with a fluorogenic assay using a fluorogenic peptide derivative of p53 (Ac-RHKK(Acetyl)-AMC) as described before[52]. The reaction was performed in HDAC assay buffer (50 mM HEPES, 150 mM NaCl, 5 mM $MgCl_2$, 1 mM TCEP and 0.2 mg/ml BSA, pH 7.4 adjusted with NaOH) with 3 % DMSO (final concentration while HDAC reaction). The compound at different concentrations was incubated with 10 nM HDAC1, or 3 nM HDAC2, or 3 nM HDAC3 (all final concentrations) for 5 min at room temperature in a 384 black fluorescence well plate. A positive control without compound and a negative control without HDAC enzyme (added buffer instead) was also done on the plate. The reaction was started with the addition of fluorogenic peptide substrate with a final concentration of 20 µM for 30 min (HDAC2 and 3) or 90 min (HDAC1). The reaction

was stopped by addition of 0.5 mg/ml Trypsin (final concentration) and 20 µM SAHA dissolved in 1 mM HCl and incubated for 1 h. The fluorescence intensity readout was performed with an Envision 2104 Multilabel Plate Reader (PerkinElmer, Waltham, MA, USA) with λ_{Ex} = 380 ± 10 nm and λ_{Em} = 430 ± 8 nm. The fluorescence intensity was normalized using the positive control as 100 % and the negative control as 0 %. A nonlinear regression analysis was done to determine the IC_{50} value.

The activity testing for HDAC11 was done as described before[43] with a substrate concentration of 15 µM and a HDAC11 concentration of 20 nM in HDAC11 assay buffer (20 mM HEPES, 70 µM TCEP and 2 mg/ml BSA, pH 7.4 adjusted with NaOH). The enzyme inhibition of HDAC8 was determined by using a reported continuous fluorescence assay[44]. The compound at different concentrations and HDAC8 (1.5 nM final concentration) were incubated in HDAC assay buffer for 5 min at room temperature. The reaction was started with the addition of substrate (Abz-SRGK(thio-TFA)FFRR-NH_2) with a concentration of 50 µM. Product formation was measured via increasing fluorescence intensity at λ_{Ex} = 330 ± 75 nm and λ_{Em} = 430 ± 8 nm. The determination of the inhibitory constant (K_i) for HDAC8 was done using the same assay with varying substrate (10-70 µM) and varying inhibitor concentrations and a HDAC8 concentration of 2 nM. The reaction was started with the addition of substrate. The slope of the Lineweaver-Burk-Plot was plotted versus the inhibitor concentration and the intercept with the abscissa represent the negative K_i value.

6. Cytotoxicity studies in HEK293 cells

HEK293 cells (DSMZ Braunschweig, ACC305) were incubated at 37 °C in a humidified incubator with 5% CO_2 in Dulbecco's modified Eagle medium (DMEM)

supplemented with 10% FCS and 5 mM glutamine. The cells were seeded out at 1.5 × 10^3 cells per well in a 96-well cell culture plate (TPP, Switzerland). All tested compounds were added immediately to the medium at 50 μM or increasing concentrations to determine IC_{50} values. After 24 h, Alamar Blue reagent (Invitrogen, CA) was added according to the manufacturer's instructions and incubated again for 21 h before the samples were analyzed. Detection of the viable cells which convert the resazurine of reagent into the high fluorescent resorufin was performed by using a FLUOstar OPTIMA microplate reader (BMG Labtec) with the following filter set: Ex 560 nm/Em 590 nm.

The measurements were performed in triplicate, and data are the mean with SD. As a positive control daunorubicin was used.

7. *In vitro* HDAC8 inhibitory activity in Jurkat T cells

Human Jurkat T lymphocytes were treated with different HDAC8 inhibitors at different concentrations for various time points, followed by mRNA and protein expression analyses by RT-qPCR and Western blot, respectively.

7.1 RNA extraction and RT-qPCR

Total RNA was extracted by using TRIzol reagent (Invitrogen). The quality and quantity of total RNA were determined by measuring absorbance at 260 nm/280 nm using NanoDrop ND-2000 (NanoDrop Technologies). One microgram of RNA was reverse transcribed to cDNA using the Reverse Transcription Master Kit (Takara) according to the manufacturer's instructions. qRT-PCR analysis was performed with SYBR green (SYBR Premix Ex Taq II, Takara) in a QuantStudio 7 Flex Real-Time PCR System (Applied Biosystems). *GAPDH* was used as an internal control. Samples were run in technical triplicates. The RT-qPCR primers are listed in Table S1.

7.2 Western blot

Protein lysates from fresh cells or tissues were prepared using lysis buffer [50 mM tris-HCl (pH 7.5), 150 mM NaCl, 1% NP-40, 0.5 % Na-deoxycholate] containing Halt Protease and Phosphatase Inhibitor Cocktail (Thermo Fisher Scientific). Protein concentration was determined by DC Protein Assay (Bio-Rad). Ten to 40 μg of protein was resolved by 10% SDS-polyacrylamide gel electrophoresis and electroblotted onto equilibrated nitrocellulose membrane (Bio-Rad Laboratories). Membranes were incubated with primary antibodies at 4°C overnight, followed by secondary antibodies for 2 h at room temperature. Antibody-antigen complexes were detected by enhanced chemiluminescence (GE Healthcare Life Sciences). Signals were quantified by ImageJ software and defined as the ratio of target protein relative to GAPDH or H3.

8. *In vivo* studies

Six- to 8-week-old C57BL/6 mice were used for in vivo experiments. All animal experiments were carried out in accordance with the guidelines approved by the Animal Experimentation Ethics Committee of The Chinese University of Hong Kong (CUHK-AEEC) and Committee on the Use of Live Animals in Teaching and Research of the University of Hong Kong (HKU-CULATR). Mice were obtained and housed at Laboratory Animal Services Centre of CUHK or Laboratory Animal Unit of HKU under specific pathogen–free conditions. To determine the function of **7d**, 100 μl of **7d** (5, 10, 25 mg/kg) or vehicle control (30% PEG400 + 0.5% Tween 80 + 5 % propylene glycol) was administered by intraperitoneal injection 5 days/week for 2 weeks. All mice were euthanized at 2 weeks after drug treatment. The spleen was collected for primary cell isolation and subsequent immune profiling analysis by multicolor flow cytometry as well as for RT-qPCR.

a) Flow cytometry

Splenocytes were isolated and followed by red cell lysis with Ammonium-Chloride-Potassium (ACK) lysis buffer (155 mM NH4Cl, 12 mM $NaHCO_3$, and 0.1 mM EDTA) as described previously[53]. For cell surface staining, single cells were incubated in 100 µl fluorescence-activated cell sorting staining buffer [1× PBS with 5% fetal bovine serum (FBS)] with antibodies at the optimal dilution according to the manufacturer's instructions for 20 min at room temperature. Flow cytometry data were acquired by FACSAria Fusion (BD Biosciences) and analyzed by FlowJo software (Tree Star). Antibodies used for flow cytometry have been specified in Table S2.

b) Toxicity evaluation

To determine potential toxicity-associated tissue damage caused by **7d**, the internal organs including heart, kidney, liver, lung, spleen and thymus were weighted and fixed in 10 % formalin for subsequent paraffin embedding. Five paraffin sections per each organ were stained with hematoxylin and eosin (H&E).

9. Characterization data of key intermediates and final compounds.

9.1 Synthesis and characterization of 7a-d.

The intermediate **2a-d** were synthesized according to method IA using 4-iodobenzohydrazide and aldehyde (*n*-propanal, *n*-butyraldehyde, *n*-pentanal, *n*-hexanal), followed by Boc-deprotection through method IIIB to give **3a-d** (**Scheme 1**).

N'-butyl-4-iodobenzohydrazide (2b) was white solid in 87 % yield. m/z ($APCI^+$) 319.1 $(M+H)^+$, 637.3 $(2M+H)^+$. ^1H NMR (400 MHz, DMSO-d_6) δ 10.04 (d, *J* = 3.7

Hz, 1H), 7.87 – 7.79 (m, 2H), 7.61 – 7.55 (m, 2H), 5.05 (s, 1H), 2.76 (s, 2H), 1.45 – 1.28 (m, 4H), 0.87 (t, *J* = 7.2 Hz, 3H).

Tert-butyl 2-(4-iodobenzoyl)-1-propylhydrazinecarboxylate (3a) was white solid in 81 % yield. ^{1}H NMR (400 MHz, $CDCl_3$) δ 8.22 (s, 1H), 7.77 (s, 2H), 7.49 (d, *J* = 8.4 Hz, 2H), 3.59 – 3.50 (m, 2H), 1.62 (dt, *J* = 14.7, 7.4 Hz, 2H), 1.47 (s, 9H), 0.93 (t, *J* = 7.4 Hz, 3H).

Tert-butyl 2-(4-iodobenzoyl)-1-pentylhydrazinecarboxylate (3c) was white solid in 63% yield. ^{1}H NMR (500 MHz, DMSO-d_6) δ 10.56 (s, 1H), 7.88 (d, *J* = 8.4 Hz, 2H), 7.66 – 7.55 (m, 2H), 3.39 (s, 2H), 1.43 (dd, *J* = 25.7, 16.3 Hz, 6H), 1.29 (d, *J* = 20.6 Hz, 9H), 0.85 (s, 3H).

Tert-butyl 1-hexyl-2-(4-iodobenzoyl)hydrazinecarboxylate (3d) was white solid in 63% yield. ^{1}H NMR (500 MHz, DMSO-d_6) δ 10.54 (s, 1H), 7.87 (d, *J* = 8.4 Hz, 2H), 7.66 – 7.56 (m, 2H), 3.40 (s, 2H), 1.54 – 1.39 (m, 6H), 1.28 (d, *J* = 31.0 Hz, 11H), 0.84 (d, *J* = 6.6 Hz, 3H).

Tert-butyl 2-(4'-((((benzyloxy)carbonyl)amino)methyl)-[1,1'-biphenyl]-4-carbonyl)-1-propylhydrazinecarboxylate (4): Synthesized according to method II using (4-((((benzyloxy)carbonyl)amino)methyl)phenyl)boronic acid **(11)** and iodobenzene **(3a)** giving compound **4** as white solid (yield: 91 %). ^{1}H NMR (400 MHz, $CDCl_3$) δ 7.85 (d, *J* = 7.8 Hz, 2H), 7.70 – 7.61 (m, 3H), 7.57 (d, *J* = 8.0 Hz, 2H), 7.49 – 7.44 (m, 1H), 7.37 (dd, *J* = 12.0, 7.9 Hz, 5H), 5.16 (s, 2H), 4.44 (d, *J* = 6.0 Hz, 2H), 3.58 (t, *J* = 7.3 Hz, 2H), 1.65 (dd, *J* = 14.6, 7.3 Hz, 2H), 1.48 (s, 9H), 0.95 (t, *J* = 7.4 Hz, 3H).

Tert-butyl 2-(4'-(aminomethyl)-[1,1'-biphenyl]-4-carbonyl)-1-propylhydrazine-carboxylate (5): Synthesized according to method III D using compound **4** to give *5* as colorless oil (yield: 80 %). m/z (APCI$^+$) 328.5 (M-tBu+2H)$^+$, 384.7 (M+H)$^+$.

***N*-((4'-(2-propylhydrazinecarbonyl)-[1,1'-biphenyl]-4-yl)methyl)acetamide (7a)**:

compound **5** was reacted with acetyl chloride following method IVC2 to yield tert-butyl **2-(4'-(acetamidomethyl)-[1,1'-biphenyl]-4-carbonyl)-1-propylhydrazine-carboxylate** (**6**) (yield: 69 %) which was converted to **7a** using method IIIB (**Scheme 1**).

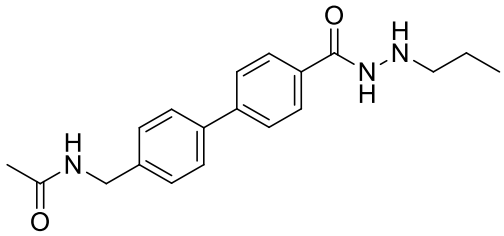

White solid (yield 87 %).

^{1}H NMR (500 MHz, DMSO-d$_6$) δ 10.05 (d, *J* = 6.0 Hz, 1H), 8.37 (t, *J* = 5.9 Hz, 1H), 7.94 – 7.88 (m, 2H), 7.75 – 7.71 (m, 2H), 7.69 – 7.64 (m, 2H), 7.35 (d, *J* = 8.4 Hz, 2H), 5.11 (dd, *J* = 11.6, 5.6 Hz, 1H), 4.29 (d, *J* = 5.9 Hz, 2H), 2.76 (dd, *J* = 12.6, 6.9 Hz, 2H), 1.88 (s, 3H), 1.51 – 1.43 (m, 2H), 0.91 (t, *J* = 7.4 Hz, 3H).

^{13}C NMR (126 MHz, DMSO-d$_6$) δ 169.61, 165.37, 142.97, 140.04, 138.09, 132.37, 128.39, 128.13, 127.19, 126.81, 53.58, 42.27, 23.03, 21.32, 12.13.

HRMS calculated for $C_{19}H_{24}N_3O_2^+$ (M+H): 326.1863, found: 326.1858.

HPLC: rt = 5.96 min (purity 98 %).

7b-d were synthesized starting from **3b-d** using method II and followed by a Boc-deprotection step using method IIIB to give **7b-d** (**Scheme 1**).

***N*-((4'-(2-butylhydrazinecarbonyl)-[1,1'-biphenyl]-4-yl)methyl)acetamide (7b)**:

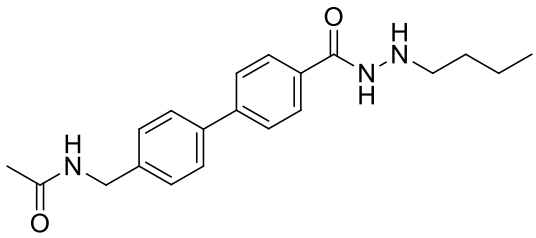

White solid (yield: 83 %).

^{1}H NMR (400 MHz, DMSO-d_6) δ 10.05 (s, 1H), 8.37 (s, 1H), 7.97 – 7.52 (m, 6H), 7.35 (d, *J* = 7.4 Hz, 2H), 5.13 (s, 1H), 4.28 (d, *J* = 5.1 Hz, 2H), 2.78 (d, *J* = 6.3 Hz, 2H), 1.88 (s, 3H), 1.56 – 1.24 (m, 4H), 0.88 (t, *J* = 6.9 Hz, 3H).

^{13}C NMR (101 MHz, DMSO-d_6) δ 169.61, 165.36, 142.97, 140.03, 138.09, 132.36, 128.39, 128.12, 127.18, 126.80, 51.38, 42.27, 30.26, 23.02, 20.29, 14.36.

HRMS calculated for $C_{20}H_{26}N_3O_2^+$ (M+H): 340.2020, found: 340.202.

HPLC: rt = 10.94 min (purity 95 %).

***N*-((4'-(2-pentylhydrazinecarbonyl)-[1,1'-biphenyl]-4-yl)methyl)acetamide (7c)**:

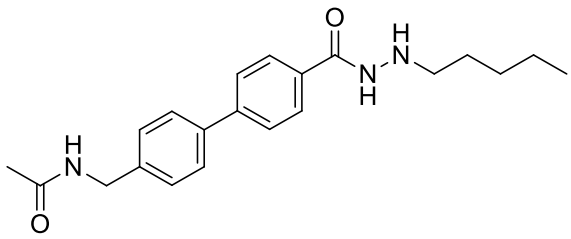

white solid (yield: 81 %).

^{1}H NMR (400 MHz, DMSO-d_6) δ 10.03 (s, 1H), 8.36 (t, *J* = 5.7 Hz, 1H), 7.89 (d, *J* = 8.3 Hz, 2H), 7.69 (dd, *J* = 25.0, 8.2 Hz, 4H), 7.34 (d, *J* = 8.1 Hz, 2H), 5.07 (s, 1H), 4.28 (d, *J* = 5.9 Hz, 2H), 2.77 (t, *J* = 7.1 Hz, 2H), 1.87 (s, 3H), 1.25 – 1.50 (m, 6H), 0.87 (t, *J* = 6.9 Hz, 3H).

^{13}C NMR (101 MHz, DMSO-d_6) δ 169.59, 165.34, 142.96, 140.03, 138.08, 132.36, 128.38, 128.11, 127.18, 126.80, 51.66, 42.26, 29.33, 27.76, 23.03, 22.50, 14.38.

HRMS calculated for $C_{21}H_{28}N_3O_2^+$ (M+H): 354.2176, found: 354.2176.

HPLC: rt = 11.80 min (purity 98 %).

***N*-((4'-(2-hexylhydrazinecarbonyl)-[1,1'-biphenyl]-4-yl)methyl)acetamide (7d)**:

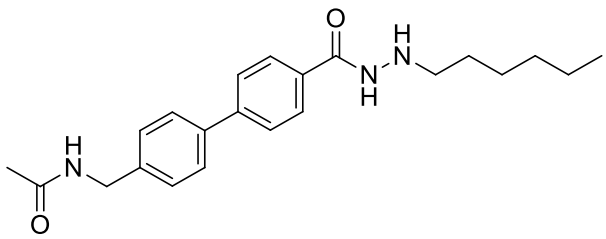

White solid (yield: 80 %).

^{1}H NMR (400 MHz, DMSO-d_6) δ 10.02 (d, *J* = 5.7 Hz, 1H), 8.35 (t, *J* = 5.9 Hz, 1H), 7.88 (d, *J* = 8.5 Hz, 2H), 7.72 (d, *J* = 8.4 Hz, 2H), 7.66 (d, *J* = 8.3 Hz, 2H), 7.34 (d, *J*

= 8.3 Hz, 2H), 5.06 (dd, *J* = 11.8, 6.2 Hz, 1H), 4.27 (d, *J* = 5.9 Hz, 2H), 2.77 (dd, *J* = 12.3, 6.8 Hz, 2H), 1.87 (s, 3H), 1.48 – 1.40 (m, 2H), 1.36 – 1.23 (m, 6H), 0.85 (t, *J* = 6.9 Hz, 3H).

^{13}C NMR (101 MHz, DMSO-d_6) δ 169.58, 165.33, 142.95, 140.03, 138.07, 132.35, 128.38, 128.11, 127.18, 126.80, 51.70, 42.26, 31.68, 28.06, 26.80, 23.02, 22.53, 14.38.

HRMS calculated for $C_{22}H_{30}N_3O_2^+$ (M+H): 368.2333, found: 368.2333.

HPLC: rt = 12.70 min (purity 100 %).

9.2 Synthesis and characterization of 7e,f.

4-((((Benzyloxy)carbonyl)amino)methyl)benzoic acid (13): see method IIIC in a 90 % yield. m/z (APCI$^+$) 286.4 (M+H)$^+$. ^{1}H NMR (400 MHz, DMSO-d_6) δ 12.84 (s, 1H), 7.88 (d, *J* = 8.2 Hz, 3H), 7.41 – 7.26 (m, 7H), 5.04 (s, 2H), 4.26 (d, *J* = 6.2 Hz, 2H).

Benzyl 4-(hydrazinecarbonyl)benzylcarbamate (14): see method IVB in a 64 % yield. ^{1}H NMR (400 MHz, DMSO-d_6) δ 9.69 (s, 1H), 7.85 (t, *J* = 5.9 Hz, 1H), 7.75 (d, *J* = 8.1 Hz, 2H), 7.41 – 7.13 (m, 7H), 5.03 (s, 2H), 4.44 (s, 2H), 4.23 (d, *J* = 6.2 Hz, 2H).

Benzyl 4-(2-propylhydrazinecarbonyl)benzylcarbamate (15a) and **benzyl 4-(2-hexylhydrazinecarbonyl)benzylcarbamate (15b)**: Synthesized according to method IB or IC using intermediate **14** and *n*-propanal or *n*-hexanal to give **15a** and **15b**. **15a**

was white solid (yield: 75%). m/z (APCI$^+$) 342.8 $(M+H)^+$; **15b** was white solid (yield: 65%). ^{1}H NMR (400 MHz, DMSO-d_6) δ 9.93 (s, 1H), 7.85 (t, *J* = 6.2 Hz, 1H), 7.74 (d, *J* = 8.3 Hz, 2H), 7.39 – 7.27 (m, 7H), 5.10 – 4.96 (m, 3H), 4.23 (d, *J* = 6.2 Hz, 2H), 2.75 (t, *J* = 7.0 Hz, 2H), 1.47 – 1.38 (m, 2H), 1.18 – 1.35(m, 6H), 0.88 – 0.82 (m, 3H).

Tert-butyl 2-(4-((((benzyloxy)carbonyl)amino)methyl)benzoyl)-1-propyl-hydrazinecarboxylate (16a) and **tert-butyl 2-(4-((((benzyloxy)carbonyl)amino)methyl)benzoyl)-1-hexylhydrazinecarboxylate (16b)**: Synthesized through method IIIA using **15a** and **15b**. **16a** was white solid (yield: 96 %). ^{1}H NMR (400 MHz, $CDCl_3$) δ 7.95 (s, 1H), 7.74 (d, *J* = 7.7 Hz, 2H), 7.45 – 7.27 (m, 7H), 5.15 (s, 2H), 4.43 (d, *J* = 6.0 Hz, 2H), 3.59 – 3.52 (m, 2H), 1.62 (dd, *J* = 14.6, 7.3 Hz, 2H), 1.46 (s, 9H), 0.94 (t, *J* = 7.4 Hz, 3H); **16b** was white semisolid (yield: 79 %).

7e and **7f** were synthesized starting from **16a** and **16b** using method IIID and followed by an acetylation step using method IVC2 to give **18a** and **18b** which were finally converted to **7e** and **7f** through method IIIB (**Scheme 2**).

***N*-(4-(2-propylhydrazinecarbonyl)benzyl)acetamide (7e)**:

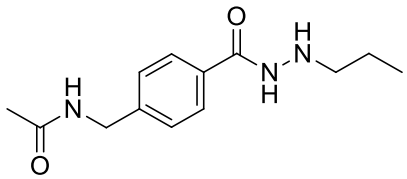

White solid (yield: 54 %).

^{1}H NMR (500 MHz, DMSO-d_6) δ 9.97 (s, 1H), 8.40 (t, *J* = 5.5 Hz, 1H), 7.76 (d, *J* = 8.2 Hz, 2H), 7.30 (d, *J* = 8.1 Hz, 2H), 4.27 (d, *J* = 5.9 Hz, 2H), 2.74 (t, *J* = 7.0 Hz, 2H), 2.49 (s, 1H), 1.87 (s, 3H), 1.49 – 1.41 (m, 2H), 0.89 (t, *J* = 7.4 Hz, 3H).

^{13}C NMR (126 MHz, DMSO-d_6) δ 169.73, 165.56, 143.42, 132.12, 127.49, 127.42, 53.55, 42.28, 22.98, 21.29, 12.09.

HRMS calculated for $C_{13}H_{19}N_3O_2Na^+$ (M+H): 272.1369, found: 272.1367.

HPLC: rt = 2.18 min (purity 97 %).

***N*-(4-(2-hexylhydrazinecarbonyl)benzyl)acetamide (7f)**:

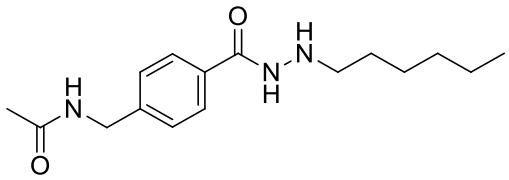

White solid (yield: 74 %).

^{1}H NMR (500 MHz, DMSO-d_6) δ 9.95 (s, 1H), 8.37 (t, *J* = 5.8 Hz, 1H), 7.76 (d, *J* = 8.1 Hz, 2H), 7.30 (d, *J* = 8.0 Hz, 2H), 5.04 (s, 1H), 4.28 (d, *J* = 6.0 Hz, 2H), 2.76 (t, *J* = 7.1 Hz, 2H), 1.88 (s, 3H), 1.47 – 1.40 (m, 2H), 1.35 – 1.23 (m, 6H), 0.86 (t, *J* = 6.8 Hz, 3H).

^{13}C NMR (126 MHz, DMSO-d_6) δ 169.67, 165.54, 143.43, 132.16, 127.49, 127.43, 51.69, 42.28, 31.68, 28.06, 26.80, 23.01, 22.53, 14.39.

HRMS calculated for $C_{32}H_{51}N_6O_4^+$ (2M+H): 583.3972, found: 583.3962.

HPLC: rt = 10.44 min (purity 99 %).

9.3 Synthesis and characterization of 7g,h

7g and **7h** were synthesized starting from **ethyl 3-aminobenzoate (19a)** and **ethyl 3-amino-4-methylbenzoate (19b)** using method VA and followed by method IVA2 to give hydrazides (**21a**,**b)** which were finally mono-alkylated using *n*-hexanal through method IC to afford **7g** and **7h** (**Scheme 3**).

3-(Benzylamino)-*N*'-hexylbenzohydrazide (7g):

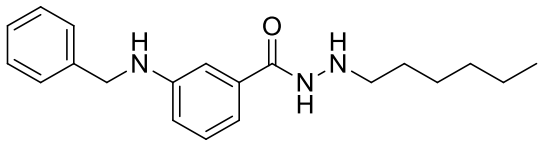

Colorless semisolid (yield: 30 %).

^{1}H NMR (400 MHz, $CDCl_3$) δ 7.37 – 7.26 (m, 5H), 7.19 (t, J = 7.9 Hz, 1H), 7.09 – 7.05 (m, 1H), 6.98 (d, J = 7.6 Hz, 1H), 6.73 (dd, J = 8.1, 2.4 Hz, 1H), 4.36 (s, 2H), 2.92 (t, J = 7.3 Hz, 2H), 1.57 – 1.47 (m, 2H), 1.40 – 1.24 (m, 6H), 0.89 (t, J = 6.9 Hz, 3H).

HRMS calculated for $C_{20}H_{28}N_3O^+$ (M+H): 326.2227, found: 326.223.

HPLC: rt = 13.58 min (purity 97 %).

3-(Benzylamino)-*N*'-hexyl-4-methylbenzohydrazide (7h):

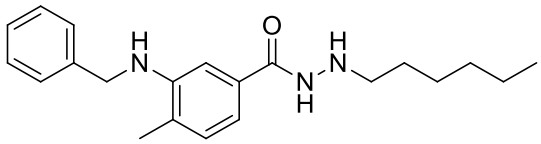

White solid (yield: 29 %).

^{1}H NMR (400 MHz, $CDCl_3$) δ 7.41 – 7.24 (m, 5H), 7.10 (d, J = 7.6 Hz, 1H), 7.05 (d, J = 1.6 Hz, 1H), 6.96 (dd, J = 7.6, 1.6 Hz, 1H), 4.41 (s, 2H), 2.94 – 2.85 (m, 2H), 2.18 (s, 3H), 1.56 – 1.46 (m, 2H), 1.41 – 1.23 (m, 6H), 0.89 (t, J = 6.9 Hz, 3H).

HRMS calculated for $C_{21}H_{30}N_3O^+$ (M+H): 340.2383, found: 340.238.

HPLC: rt = 14.04 min (purity 98 %).

9.4 Synthesis and characterization of 28a-m.

28a-m were prepared starting from ethyl 2-chloropyrimidine-5-carboxylate (**25**) and corresponding amine (presented in **Scheme 4)** following method VB to give intermediate **26a-m** which were reacted with hydrazine monohydate according to method IVA1 or IVA2 to yield intermediate **27a-m**. Finally, **27a-m** were mono-alkylated following method IC to yield final compounds **28a-m**.

***N*-(4-(aminomethyl)benzyl)acetamide hydrochloride (24)**: 4-(acetamidomethyl)benzylcarbamate (**23**) was synthesized according to method IVC2 using tert-butyl 4-(aminomethyl)benzylcarbamate (**22**) giving **23** as orange oil. m/z (APCI$^+$) 223.0 $(M+H)^+$, 557.2 $(2M+H)^+$. ^{1}H NMR (400 MHz, $CDCl_3$) δ 7.24 (s, 4H), 5.71 (s, 1H), 4.83 (s, 1H), 4.41 (d, *J* = 5.7 Hz, 2H), 4.29 (d, *J* = 5.7 Hz, 2H), 2.02 (s, 3H), 1.46 (s, 9H). The intermediate **23** through method IIIB was converted to compound **24** as light yellow solid (yield: 93 % over two steps).

Ethyl 2-(benzylamino)pyrimidine-5-carboxylate (26a): White solid (yield: 87 %). ^{1}H NMR (400 MHz, DMSO-d_6) δ 8.71 (d, *J* = 1.3 Hz, 2H), 8.60 (t, *J* = 6.2 Hz, 1H),

7.31 – 7.16 (m, 5H), 4.56 (d, *J* = 6.4 Hz, 2H), 4.24 (q, *J* = 7.1 Hz, 2H), 1.26 (t, *J* = 7.1 Hz, 3H).

Ethyl 2-(4-methylpiperazin-1-yl)pyrimidine-5-carboxylate (26h): White solid (yield: 90 %). ^{1}H NMR (400 MHz, DMSO-d_6) δ 8.76 (s, 2H), 4.25 (q, *J* = 7.1 Hz, 2H), 3.87 – 3.80 (m, 4H), 2.38 – 2.33 (m, 4H), 2.20 (s, 3H), 1.27 (t, *J* = 7.1 Hz, 3H).

Ethyl 2-((4-(acetamidomethyl)benzyl)amino)pyrimidine-5-carboxylate (26i): White solid (yield: 89 %). ^{1}H NMR (400 MHz, DMSO-d_6) δ 8.71 (d, J = 0.9 Hz, 2H), 8.58 (t, J = 6.4 Hz, 1H), 8.29 – 8.22 (m, 1H), 7.19 (dd, J = 26.9, 8.2 Hz, 4H), 4.52 (d, J = 6.4 Hz, 2H), 4.23 (q, J = 7.1 Hz, 2H), 4.18 (d, J = 5.8 Hz, 2H), 1.83 (s, 3H), 1.26 (t, J = 7.1 Hz, 3H).

2-(4-Methylpiperazin-1-yl)pyrimidine-5-carbohydrazide (27h): White solid (yield: 91%). ^{1}H NMR (500 MHz, DMSO-d_6) δ 9.64 (s, 1H), 8.72 (s, 2H), 4.37 (d, *J* = 66.4 Hz, 2H), 3.84 – 3.70 (m, 4H), 2.39 – 2.27 (m, 4H), 2.19 (s, 3H).

***N*-(4-(((5-(Hydrazinecarbonyl)pyrimidin-2-yl)amino)methyl)benzyl)acetamide (27i)**: White solid (yield: 70 %). ^{1}H NMR (400 MHz, DMSO-d_6) δ 9.52 (s, 1H), 8.63 (s, 2H), 8.27 – 8.20 (m, 2H), 7.19 (dd, J = 27.7, 8.1 Hz, 4H), 4.49 (d, J = 6.3 Hz, 2H), 4.37 (s, 2H), 4.18 (d, J = 5.9 Hz, 2H), 1.82 (s, 3H).

2-(Benzylamino)-*N*'-propylpyrimidine-5-carbohydrazide (28a):

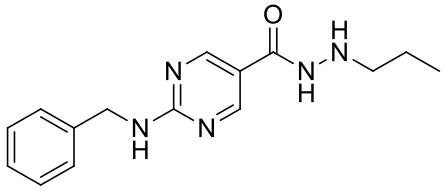

White solid (yield: 33 %).

^{1}H NMR (400 MHz, DMSO-d_6) δ 9.82 (s, 1H), 8.64 (s, 2H), 8.25 (t, *J* = 6.3 Hz, 1H), 7.32 – 7.16 (m, 5H), 4.99 (s, 1H), 4.53 (d, *J* = 6.4 Hz, 2H), 2.69 (t, *J* = 7.1 Hz, 2H), 1.41 (dt, *J* = 14.5, 7.3 Hz, 2H), 0.86 (t, *J* = 7.4 Hz, 3H).

^{13}C NMR (101 MHz,DMSO-d_6) δ 163.55, 163.28, 158.16, 157.70, 140.09, 128.68, 127.42, 127.12, 115.94, 53.57, 44.39, 21.22, 12.04.

HRMS calculated for $C_{15}H_{20}N_5O^+$ (M+H): 286.1662, found: 286.166.

HPLC: rt = 4.95 min (purity 95 %).

2-(Benzylamino)-*N*'-butylpyrimidine-5-carbohydrazide (28b)：

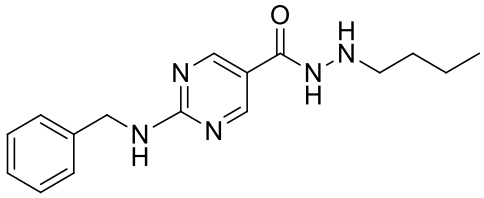

White solid (yield: 58 %).

^{1}H NMR (400 MHz, DMSO-d_6) δ 9.79 (s, 1H), 8.65 (s, 2H), 8.26 (t, *J* = 6.3 Hz, 1H), 7.32 – 7.15 (m, 5H), 5.00 (s, 1H), 4.53 (d, *J* = 6.4 Hz, 2H), 2.73 (t, *J* = 7.0 Hz, 2H), 1.44 – 1.26 (m, 4H), 0.86 (t, *J* = 7.2 Hz, 3H).

^{13}C NMR (101 MHz, DMSO-d_6) δ 163.50, 163.33, 158.11, 157.68, 140.16, 128.66, 127.44, 127.09, 115.98, 51.40, 44.41, 30.22, 20.25, 14.33.

HRMS calculated for $C_{16}H_{22}N_5O^+$ (M+H): 300.1819, found: 300.182.

HPLC: rt = 11.53 min (purity 98 %).

2-(Phenethylamino)-*N*'-propylpyrimidine-5-carbohydrazide (28c):

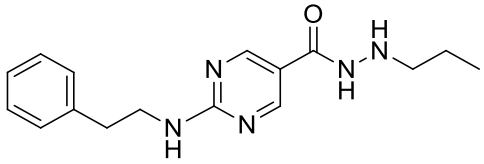

White solid (yield: 53 %).

^{1}H NMR (400 MHz, DMSO-d_6) δ 9.79 (s, 1H), 8.66 (d, *J* = 18.8 Hz, 2H), 7.79 (t, *J* = 5.6 Hz, 1H), 7.29 – 7.14 (m, 5H), 5.01 (s, 1H), 3.52 (dd, *J* = 14.0, 6.6 Hz, 2H), 2.82 (t, *J* = 7.3 Hz, 2H), 2.71 (t, *J* = 7.0 Hz, 2H), 1.48 – 1.37 (m, 2H), 0.88 (t, *J* = 7.4 Hz, 3H).

^{13}C NMR (101 MHz, DMSO-d_6) δ 163.58, 163.19, 157.95, 157.76, 139.92, 129.09, 128.72, 126.47, 115.61, 53.62, 42.77, 35.23, 21.29, 12.08.

HRMS calculated for $C_{16}H_{22}N_5O^+$ (M+H): 300.1819, found: 300.182.

HPLC: rt = 5.75 min (purity 99 %).

2-((Naphthalen-1-ylmethyl)amino)-*N*'-propylpyrimidine-5-carbohydrazide (28d):

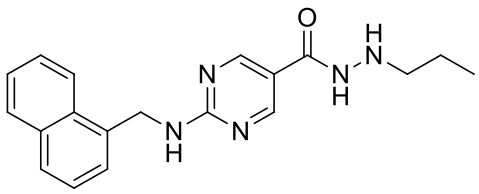

White solid (yield: 67 %).

^{1}H NMR (400 MHz, DMSO-d_6) δ 9.80 (s, 1H), 8.67 (s, 2H), 8.32 (t, *J* = 6.0 Hz, 1H), 8.16 – 8.11 (m, 1H), 7.95 – 7.90 (m, 1H), 7.83 – 7.78 (m, 1H), 7.57 – 7.50 (m, 2H), 7.45 – 7.40 (m, 2H), 5.00 (d, *J* = 6.1 Hz, 3H), 2.70 (t, *J* = 7.1 Hz, 2H), 1.47 – 1.37 (m, 2H), 0.88 (t, *J* = 7.4 Hz, 3H).

^{13}C NMR (101 MHz, DMSO-d_6) δ 163.50, 163.33, 158.18, 157.74, 135.06, 133.73, 131.30, 128.96, 127.71, 126.59, 126.18, 125.84, 125.03, 123.80, 116.04, 53.59, 42.58, 21.29, 12.09.

HRMS calculated for $C_{19}H_{22}N_5O^+$ (M+H): 336.1819, found: 336.1818.

HPLC: rt = 11.64 min (purity 94 %).

2-((2-Chlorobenzyl)amino)-*N*'-propylpyrimidine-5-carbohydrazide (28e):

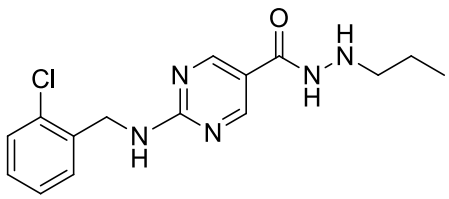

White solid (yield: 64 %).

^{1}H NMR (400 MHz, DMSO-d_6) δ 9.81 (s, 1H), 8.66 (d, *J* = 12.2 Hz, 2H), 8.26 (t, *J* = 6.1 Hz, 1H), 7.45 – 7.39 (m, 1H), 7.29 – 7.22 (m, 3H), 5.01 (s, 1H), 4.59 (d, *J* = 6.2 Hz, 2H), 2.70 (t, *J* = 6.9 Hz, 2H), 1.49 – 1.36 (m, 2H), 0.87 (t, *J* = 7.4 Hz, 3H).

^{13}C NMR (101 MHz, DMSO-d_6) δ 163.43, 163.28, 158.21, 157.70, 136.94, 132.37, 129.56, 128.86, 128.60, 127.54, 116.37, 53.58, 42.51, 21.28, 12.08.

HRMS calculated for $C_{15}H_{19}ClN_5O^+$ (M+H): 320.1273, found: 320.1271.

HPLC: rt = 11.93 min (purity 96 %).

2-((4-Chlorobenzyl)amino)-*N*'-propylpyrimidine-5-carbohydrazide (28f):

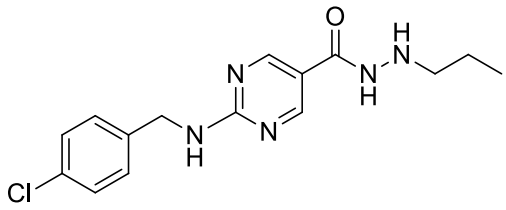

White solid (yield: 66 %).

^{1}H NMR (400 MHz, DMSO-d_6) δ 9.79 (s, 1H), 8.65 (s, 2H), 8.28 (t, *J* = 6.3 Hz, 1H), 7.36 – 7.27 (m, 4H), 5.01 (s, 1H), 4.51 (d, *J* = 6.4 Hz, 2H), 2.70 (t, *J* = 7.1 Hz, 2H), 1.47 – 1.37 (m, 2H), 0.87 (t, *J* = 7.4 Hz, 3H).

^{13}C NMR (101 MHz, DMSO-d_6) δ 163.44, 163.23, 158.14, 157.66, 139.25, 131.63, 129.33, 128.62, 116.16, 53.58, 43.81, 21.28, 12.08.

HRMS calculated for $C_{15}H_{18}Cl_2N_5O^+$ (M+H): 320.1273, found: 320.1272.

HPLC: rt = 11.90 min (purity 96 %)

2-((2,5-Dichlorobenzyl)amino)-*N*'-propylpyrimidine-5-carbohydrazide (28g):

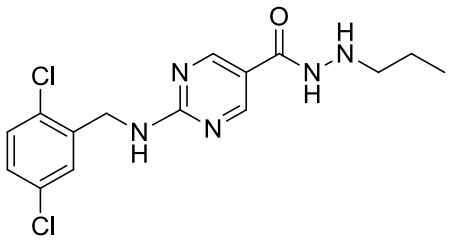

White solid (yield: 72 %).

^{1}H NMR (400 MHz, DMSO-d_6) δ 9.81 (s, 1H), 8.67 (d, *J* = 9.7 Hz, 2H), 8.28 (t, *J* = 6.1 Hz, 1H), 7.57 (d, *J* = 2.0 Hz, 1H), 7.37 – 7.26 (m, 2H), 5.01 (s, 1H), 4.55 (d, *J* = 6.1 Hz, 2H), 2.70 (t, *J* = 6.4 Hz, 2H), 1.48 – 1.36 (m, 2H), 0.87 (t, *J* = 7.4 Hz, 3H).

^{13}C NMR (101 MHz, DMSO-d_6) δ 163.38, 163.17, 158.24, 157.71, 136.22, 133.29, 132.48, 130.06, 129.00, 127.70, 116.51, 53.57, 42.18, 21.28, 12.07.

HRMS calculated for $C_{15}H_{18}Cl_2N_5O^+$ (M+H): 354.0883, found: 354.0883.

HPLC: rt = 13.43 min (purity 97 %)

2-(4-Methylpiperazin-1-yl)-*N*'-propylpyrimidine-5-carbohydrazide (28h):

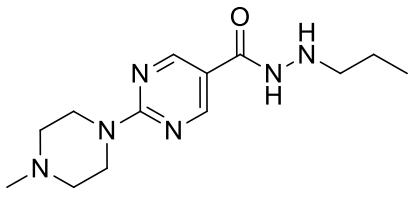

White solid (yield: 44 %).

^{1}H NMR (500 MHz,DMSO-d_6) δ 9.92 (s, 1H), 8.75 (s, 2H), 3.89 (s, 4H), 2.73 (s, 2H), 2.63 (s, 4H), 2.38 (s, 3H), 1.44 (dd, *J* = 14.2, 7.0 Hz, 2H), 0.89 (t, *J* = 7.3 Hz, 3H).

^{13}C NMR (126 MHz, DMSO-d_6) δ 163.22, 161.77, 160.07, 157.80, 53.91, 53.57, 44.97, 42.87, 21.31, 12.09.

HRMS calculated for $C_{13}H_{23}N_6O^+$ (M+H): 279.1928, found: 279.1926.

HPLC: rt = 5.07 min (purity 98 %).

***N*-(4-(((5-(2-propylhydrazinecarbonyl)pyrimidin-2-yl)amino)methyl)benzyl)-acetamide (28i)**:

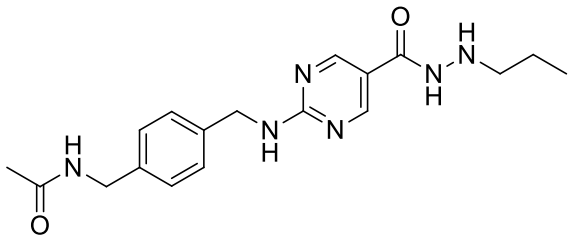

White solid (yield: 66 %).

^{1}H NMR (400 MHz, DMSO-d_6) δ 9.84 (s, 1H), 8.66 (s, 2H), 8.28 (dt, *J* = 12.7, 5.9 Hz, 2H), 7.19 (dd, *J* = 26.8, 8.0 Hz, 4H), 4.51 (t, *J* = 8.6 Hz, 2H), 4.18 (d, *J* = 5.9 Hz, 2H), 2.71 (s, 2H), 1.83 (s, 3H), 1.41 (dt, *J* = 14.4, 7.2 Hz, 2H), 0.87 (t, *J* = 7.4 Hz, 3H).

^{13}C NMR (101 MHz, DMSO-d_6) δ 169.50, 163.48 163.28, 158.13, 157.71, 138.63, 138.43, 127.68, 127.43, 53.56, 44.19, 42.33, 22.98, 21.28, 12.07.

HRMS calculated for $C_{18}H_{25}N_6O_2^+$ (M+H): 357.2034, found: 357.2034.

HPLC: rt = 8.54 min (purity 98 %).

***N*'-hexyl-2-((naphthalen-1-ylmethyl)amino)pyrimidine-5-carbohydrazide (28j)**:

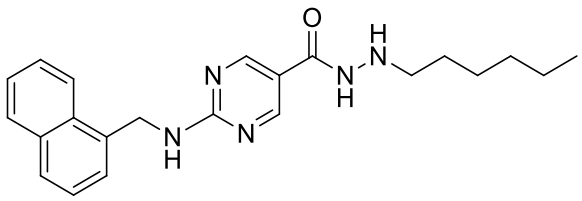

White solid (yield: 72 %).

^{1}H NMR (400 MHz, DMSO-d_6) δ 9.81 (s, 1H), 8.67 (s, 2H), 8.33 (t, *J* = 6.0 Hz, 1H), 8.13 (d, *J* = 8.6 Hz, 1H), 7.92 (dd, *J* = 6.7, 2.6 Hz, 1H), 7.83 – 7.77 (m, 1H), 7.57 – 7.40 (m, 4H), 5.00 (d, *J* = 6.0 Hz, 3H), 2.72 (t, *J* = 6.8 Hz, 2H), 1.45 – 1.36 (m, 2H), 1.34 – 1.19 (m, 6H), 0.83 (dd, *J* = 8.7, 4.7 Hz, 3H).

^{13}C NMR (101 MHz, DMSO-d_6) δ 163.50, 163.33, 158.16, 157.76, 135.06, 133.73, 131.30, 128.96, 127.71, 126.59, 126.18, 125.83, 125.03, 123.79, 116.03, 51.72, 42.58, 31.65, 28.04, 26.77, 22.52, 14.36.

HRMS calculated for $C_{22}H_{28}N_5O^+$ (M+H): 378.2288, found: 378.2290.

HPLC: rt = 14.43 min (purity 97 %)

***N'*-hexyl-2-(phenethylamino)pyrimidine-5-carbohydrazide (28k)**:

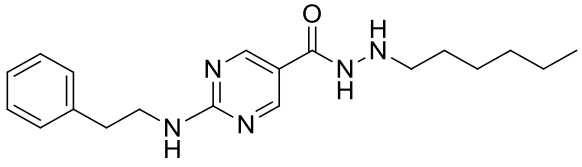

White solid (yield: 69 %).

^{1}H NMR (400 MHz, DMSO-d_6) δ 9.78 (s, 1H), 8.64 (d, *J* = 18.8 Hz, 2H), 7.79 (t, *J* = 5.7 Hz, 1H), 7.32 – 7.11 (m, 5H), 4.98 (s, 1H), 3.52 (dd, *J* = 14.4, 6.3 Hz, 2H), 2.87 –

2.79 (m, 2H), 2.73 (t, *J* = 7.0 Hz, 2H), 1.41 (dt, *J* = 14.0, 7.2 Hz, 2H), 1.35 – 1.19 (m, 6H), 0.85 (t, *J* = 6.8 Hz, 3H).

HRMS calculated for $C_{19}H_{28}N_5O^+$ (M+H): 342.2288, found: 342.2287.

HPLC: rt = 13.99 min (purity 99%)

2-(Benzylamino)-*N*'-hexylpyrimidine-5-carbohydrazide (28l):

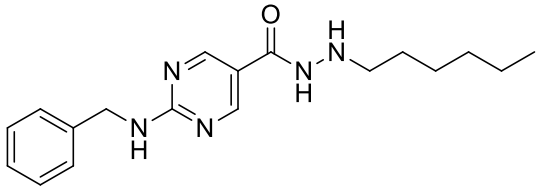

White solid (yield: 74 %).

^{1}H NMR (400 MHz, DMSO-d_6) δ 9.80 (s, 1H), 8.68 (d, *J* = 13.0 Hz, 2H), 8.27 (t, *J* = 6.3 Hz, 1H), 7.39 – 7.13 (m, 5H), 5.05 (s, 1H), 4.54 (d, *J* = 6.3 Hz, 2H), 2.73 (t, *J* = 7.0 Hz, 2H), 1.46 – 1.35 (m, 2H), 1.33 – 1.18(m, 6H), 0.83 (t, *J* = 6.7 Hz, 3H).

^{13}C NMR (101 MHz, DMSO-d_6) δ 163.50, 163.34, 158.13, 157.70, 140.16, 128.64, 127.44, 127.07, 115.98, 51.74, 44.43, 31.66, 28.05, 26.78, 22.53, 14.34.

HRMS calculated for $C_{18}H_{26}N_5O^+$ (M+H): 328.2132, found: 328.2131.

HPLC: rt = 13.59 min (purity 97 %).

***N*-(4-(((5-(2-hexylhydrazinecarbonyl)pyrimidin-2-yl)amino)methyl)benzyl)acetamide (28m)**:

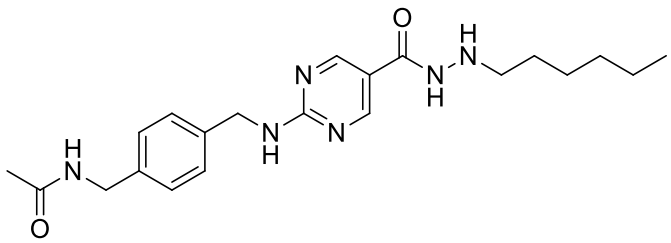

White solid (yield: 55 %).

^{1}H NMR (500 MHz, DMSO-d_6) δ 9.80 (s, 1H), 8.66 (s, 2H), 8.27 (t, *J* = 6.0 Hz, 2H), 7.21 (dd, *J* = 33.1, 7.9 Hz, 4H), 5.02 (s, 1H), 4.51 (d, *J* = 6.3 Hz, 2H), 4.20 (d, *J* = 5.9 Hz, 2H), 2.74 (t, *J* = 7.1 Hz, 2H), 1.85 (s, 3H), 1.47 – 1.38 (m, 2H), 1.34 – 1.23 (m, 6H), 0.86 (t, *J* = 6.7 Hz, 3H).

^{13}C NMR (126 MHz, DMSO-d_6) δ 169.48, 163.52, 163.30, 158.10, 157.68, 138.65, 138.45, 127.71, 127.45, 115.98, 51.74, 44.21, 42.35, 31.67, 28.06, 26.79, 23.01, 22.54, 14.38.

HRMS calculated for $C_{21}H_{31}N_6O_2^+$ (M+H): 399.2503, found: 399.2502.

HPLC: rt = 11.69 min (purity 96 %).

9.5 Synthesis and characterization of 40a-e

Benzylpiperazine dihydrochloride (33): Prepared according to method IIIB using intermediate **32**. White solid (yield: 68 %).

Ethyl 2-(4-benzylpiperazin-1-yl)pyrimidine-5-carboxylate (34): Prepared according to method VB (DIPEA = 4.5 mmol) using compound **33**. White solid (yield: 97%). m/z (APCI$^+$) 327.4 (M+H)$^+$. ^{1}H NMR (400 MHz, DMSO-d_6) δ 8.75 (s, 2H),

7.34 – 7.22 (m, 5H), 4.24 (q, *J* = 7.1 Hz, 2H), 3.89 – 3.77 (m, 4H), 3.50 (s, 2H), 2.47 – 2.38 (m, 4H), 1.27 (t, *J* = 7.1 Hz, 3H).

2-(4-Benzylpiperazin-1-yl)-N'-propylpyrimidine-5-carbohydrazide (36a) and **2-(4-benzylpiperazin-1-yl)-N'-hexylpyrimidine-5-carbohydrazide (36b)**:

Intermediate **34** was converted to 2-(4-benzylpiperazin-1-yl)pyrimidine-5-carbohydrazide (**35**) using method IVA1 followed by a hydrazide mono-alkylation with *n*-propanal or *n*-hexanal through method IC to yield **36a** and **36b**.

36a was white solid (yield: 86 %). ^{1}H NMR (400 MHz, DMSO-d_6) δ 9.83 (d, J = 5.4 Hz, 1H), 8.70 (s, 2H), 7.35 – 7.21 (m, 5H), 5.01 (d, J = 5.5 Hz, 1H), 3.84 – 3.76 (m, 4H), 3.50 (s, 2H), 2.71 (dd, J = 11.8, 6.7 Hz, 2H), 2.44 – 2.37 (m, 4H), 1.42 (dt, J = 14.5, 7.2 Hz, 2H), 0.88 (t, J = 7.4 Hz, 3H);

36b was white solid (yield: 36%). ^{1}H NMR (400 MHz, DMSO-d_6) δ 9.83 (d, J = 5.9 Hz, 1H), 8.70 (s, 2H), 7.35 – 7.22 (m, 5H), 4.98 (d, J = 5.8 Hz, 1H), 3.85 – 3.73 (m, 4H), 3.50 (s, 2H), 2.73 (dd, J = 12.3, 6.5 Hz, 2H), 2.43 – 2.36 (m, 4H), 1.41 (dt, J = 14.0, 6.9 Hz, 2H), 1.35 – 1.23 (m, 6H), 0.84 (t, J = 6.8 Hz, 3H).

To prepare final compounds **40a-e,** 2-(piperazin-1-yl)-*N*'-propylpyrimidine-5-carbohydrazide (**38a**) and *N*'-hexyl-2-(piperazin-1-yl)pyrimidine-5-carbohydrazide (**38b**) were synthesized starting from **36a** and **36b** using method IIIA and followed by a Benzyl-deprotection step according to method IIIF. These two intermediates (**38a**,**b**) were reacted with indole-3-carbaldehyde or 1-methyl-indole-3-carbaldehyde according to method VII to give tert-butyl 2-(2-(4-((1*H*-indol-3-yl)methyl)piperazin-1-yl)pyrimidine-5-carbonyl)-1-propylhydrazinecarboxylate (**39a**), tert-butyl 2-(2-(4-

((1*H*-indol-3-yl)methyl)piperazin-1-yl)pyrimidine-5-carbonyl)-1-hexylhydrazinecarboxylate (**39b**) and tert-butyl 1-hexyl-2-(2-(4-((1-methyl-1*H*-indol-3-yl)methyl)piperazin-1-yl)pyrimidine-5-carbonyl)hydrazinecarboxylate (**39c**) which were converted to final compounds **40a**-**c** using the Boc-deprotection method IIIB (**Scheme 5**).

38b was reacted with 3-(2-bromoethyl)-indole or 3-(2-bromoethyl)-1-methyl-indole using method VC to yield intermediate tert-butyl 2-(2-(4-(2-(1*H*-indol-3-yl)ethyl)piperazin-1-yl)pyrimidine-5-carbonyl)-1-hexylhydrazinecarboxylate (**39d**) and tert-butyl 1-hexyl-2-(2-(4-(2-(1-methyl-1*H*-indol-3-yl)ethyl)piperazin-1-yl)pyrimidine-5-carbonyl)hydrazinecarboxylate (**39e**) which were converted to final compounds **40d**,**e** using the Boc-deprotection method IIIB (**Scheme 5**).

2-(4-((1*H*-indol-3-yl)methyl)piperazin-1-yl)-*N*'-propylpyrimidine-5-carbohydrazide (40a):

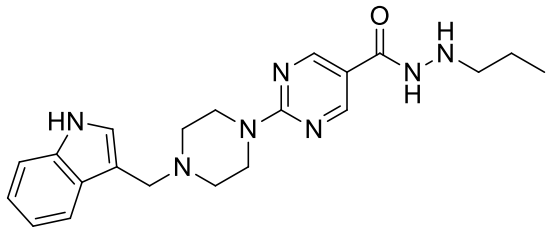

White solid (yield: 56 %).

^{1}H NMR (400 MHz, DMSO-d_6). δ 10.92 (d, *J* = 1.4 Hz, 1H), 9.84 (s, 1H), 8.71 (s, 2H), 7.64 (d, *J* = 7.8 Hz, 1H), 7.34 (d, *J* = 8.1 Hz, 1H), 7.22 (d, *J* = 2.3 Hz, 1H), 7.08 – 7.01 (m, 1H), 7.00 – 6.93 (m, 1H), 5.02 (s, 1H), 3.82 – 3.72 (m, 4H), 3.64 (s, 2H),

2.72 (t, *J* = 7.1 Hz, 2H), 2.46 – 2.34 (m, 4H), 1.48 – 1.38 (m, 2H), 0.88 (t, *J* = 7.4 Hz, 3H).

^{13}C NMR (101 MHz, DMSO-d_6) δ 162.98, 161.35, 157.27, 136.35, 127.58, 124.68, 120.93, 119.03, 118.43, 114.86, 111.34, 110.44, 53.18, 53.13, 52.25, 43.57, 20.86, 11.63.

HRMS calculated for $C_{21}H_{28}N_7O^+$ (M+H): 394.2350, found: 394.2343.

HPLC: rt = 8.77 min (purity 98 %).

2-(4-((1*H*-indol-3-yl)methyl)piperazin-1-yl)-*N*'-hexylpyrimidine-5-carbohydrazide (40b):

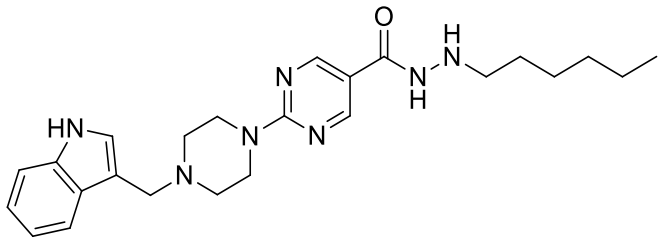

White solid (yield: 34 %).

^{1}H NMR (400 MHz, DMSO-d_6) δ 10.92 (d, *J* = 1.7 Hz, 1H), 9.84 (s, 1H), 8.72 (d, *J* = 8.1 Hz, 2H), 7.63 (d, *J* = 7.9 Hz, 1H), 7.34 (d, *J* = 8.1 Hz, 1H), 7.22 (d, *J* = 2.3 Hz, 1H), 7.01 (dtd, *J* = 15.9, 7.1, 1.1 Hz, 2H), 5.00 (s, 1H), 3.82 – 3.72 (m, 4H), 3.64 (s, 2H), 2.74 (t, *J* = 7.1 Hz, 2H), 2.46 – 2.38 (m, 4H), 1.40 (dd, *J* = 14.4, 7.3 Hz, 2H), 1.33 – 1.19 (m, 6H), 0.83 (t, *J* = 6.8 Hz, 3H).

^{13}C NMR (101 MHz, DMSO-d_6) δ 163.40, 161.79, 157.71, 136.80, 128.03, 125.12, 121.37, 119.47, 118.86, 115.30, 111.78, 110.89, 53.60, 52.70, 51.76, 44.02, 31.66, 28.06, 26.79, 22.53, 14.35.

HRMS calculated for $C_{24}H_{34}N_7O^+$ (M+H): 436.2819, found: 436.282.

HPLC: rt = 11.90 min (purity 99 %).

***N'*-hexyl-2-(4-((1-methyl-1*H*-indol-3-yl)methyl)piperazin-1-yl)pyrimidine-5-carbohydrazide (40c)**:

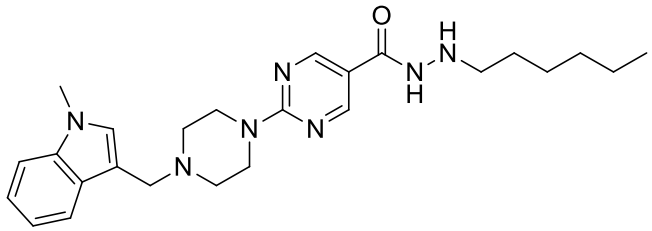

White solid (yield: 36 %).

^{1}H NMR (400 MHz, DMSO-d_6) δ 9.85 (s, 1H), 8.71 (s, 2H), 7.64 (d, *J* = 7.8 Hz, 1H), 7.35 (d, *J* = 8.2 Hz, 1H), 7.19 (s, 1H), 7.14 – 7.09 (m, 1H), 7.03 – 6.98 (m, 1H), 5.00 (s, 1H), 3.81 – 3.75 (m, 4H), 3.72 (s, 3H), 3.62 (s, 2H), 2.74 (t, *J* = 7.1 Hz, 2H), 2.46 – 2.36 (m, 4H), 1.41 (dt, *J* = 14.2, 7.0 Hz, 2H), 1.32 – 1.19 (m, 6H), 0.83 (t, *J* = 6.8 Hz, 3H).

^{13}C NMR (101 MHz, DMSO-d_6) δ 163.39, 161.7, 157.71, 137.18, 129.41, 128.37, 121.50, 119.66, 119.00, 115.31, 110.14, 109.95, 53.33, 52.65, 51.76, 44.00, 32.70, 31.66, 28.07, 26.79, 22.53, 14.35. HRMS calculated for $C_{25}H_{36}N_7O^+$ (M+H): 450.2976, found: 450.297.

HPLC: rt = 12.61 min (purity 98 %).

2-(4-(2-(1*H*-indol-3-yl)ethyl)piperazin-1-yl)-*N*'-hexylpyrimidine-5-carbohydrazide (40d):

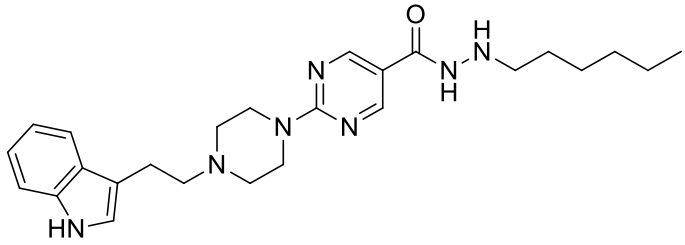

White solid (yield: 23 %).

^{1}H NMR (400 MHz, DMSO-d_6) δ 10.75 (s, 1H), 9.85 (s, 1H), 8.73 (s, 2H), 7.50 (d, J = 7.8 Hz, 1H), 7.31 (d, J = 8.1 Hz, 1H), 7.14 (s, 1H), 7.04 (t, J = 7.5 Hz, 1H), 6.95 (t, J = 7.4 Hz, 1H), 5.00 (s, 1H), 3.82 (s, 4H), 2.91 – 2.83 (m, 2H), 2.74 (t, J = 7.0 Hz, 2H), 2.66 – 2.59 (m, 2H), 2.52 (s, 4H), 1.45 – 1.37 (m, 2H), 1.34 – 1.20 (m, 6H), 0.84 (t, J = 6.8 Hz, 3H).

^{13}C NMR (101 MHz, DMSO-d_6) δ 163.38, 161.86, 157.73, 136.63, 127.67, 122.91, 121.24, 118.70, 118.56, 115.39, 112.87, 111.75, 59.16, 52.92, 51.74, 43.98, 31.66, 28.06, 26.78, 22.84, 22.53, 14.36.

HRMS calculated for $C_{25}H_{36}N_7O^+$ (M+H): 450.2976, found: 450.297.

HPLC: rt = 11.67 min (purity 96 %).

***N*'-hexyl-2-(4-(2-(1-methyl-1*H*-indol-3-yl)ethyl)piperazin-1-yl)pyrimidine-5-carbohydrazide (40e)**:

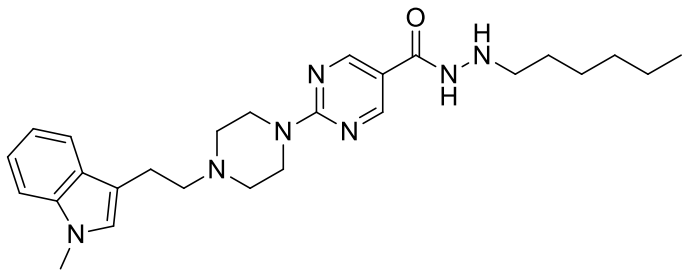

White solid (yield: 44 %).

^{1}H NMR (400 MHz, DMSO-d_6) δ 9.86 (s, 1H), 8.73 (s, 2H), 7.51 (d, *J* = 7.8 Hz, 1H), 7.33 (d, *J* = 8.2 Hz, 1H), 7.17 – 7.04 (m, 2H), 6.98 (dd, *J* = 11.0, 3.9 Hz, 1H), 5.01 (s, 1H), 3.90 – 3.78 (m, 4H), 3.70 (s, 3H), 2.91 – 2.81 (m, 2H), 2.74 (t, *J* = 7.0 Hz, 2H), 2.65 – 2.56 (m, 2H), 2.55 – 2.48 (m, 4H), 1.46 – 1.37 (m, 2H), 1.33 – 1.18 (m, 6H), 0.84 (t, *J* = 6.8 Hz, 3H).

^{13}C NMR (101 MHz, DMSO-d_6) δ 163.38, 161.86, 157.73, 137.01, 127.99, 127.35, 121.39, 118.94, 118.66, 115.38, 112.28, 109.89, 59.18, 52.92, 51.76, 43.97, 32.63, 31.66, 28.07, 26.79, 22.67, 22.53, 14.36.

HRMS calculated for $C_{26}H_{38}N_7O^+$ (M+H): 464.3132, found: 464.3126.

HPLC: rt = 12.62 min (purity 99 %).

Acknowledgements

We thank Simone Kniesa for excellent technical assistance. We are grateful to Cyril Barinka (Institute of Biotechnology of the Czech Academy of Sciences, BIOCEV, Prague, Czech Republic) for providing HDAC11 enzyme.

Conflict of interest

The authors declare that they have no known competing financial interests or personal relationships that could have appeared to influence the work reported in this paper.

Funding

This work was funded by the Deutsche Forschungsgemeinschaft (DFG) SI868/22-1 project number 46995445 (to W.S.), the Collaborative Research Fund (C4045-18W) and the Li Ka Shing Foundation (to A.S.L.C). P.S. acknowledges funding by a full scholarship from the China Scholarship Council (CSC).

Author Contributions

P.S[#] and J.W[#] contributed equally to this work. P.S. synthesized some of the compounds and wrote the manuscript. N.I. synthesized some of the compounds. M.Z. carried out the HDAC *in vitro* testing and analyzed data. E.B. and D.R. did the docking and modelling studies. F.E. carried out the cytotoxicity testing on human HEK293 cells. J.W, K.S.K, W.Y, carried out the cellular testing and in vivo study. C.R. expressed and provided HDAC8 protein for *in vitro* testing. M.S. carried out non-enzymatic stability test. W.-L.N., A.C, M.S. and W.S. designed experiments, analyzed data, and wrote the paper. All authors have given approval to the final version of the manuscript.

Supporting Information

This material is available free of charge. The Supporting Information is available free of charge on

Abbrevations used

Boc, tert-Butyloxycarbonyl; Cbz, benzyl chlorocarbonate; DCM, dichloromethan; DMSO, dimethylsulfoxie; DMEM, Dulbecco's modified eagle medium; DIPEA, diisopropylethylamine; HDAC, histone deacetylase; HCC, hepatocellular carcinoma; SMC3, structural maintenance of chromosomes protein 3; TEA, triethylamine; TFA, trifluoracetic acid; THF, tetrahydrofuran; TLC, thin layer chromatography; vdW, van der Waals.

Author Information

Corresponding Authors

*Phone: +85239439842. E-mail: alfredcheng@cunk.edu.hk

*Phone: +493455525040. E-mail: wolfgang.sippl@pharmazie.uni-halle.de

ORCID

Christophe Romier: 0000-0002-3680-935X

Mike Schutkowski: 0000-0003-0919-7076

Alfred Sze-Lok Cheng: 0000-0003-2345-6951

Wolfgang Sippl: 0000-0002-5985-9261

References

1. Gallinari, P.; Marco, S. D.; Jones, P.; Pallaoro, M.; Steinkühler, C., HDACs, histone deacetylation and gene transcription: from molecular biology to cancer therapeutics. *Cell Research* **2007,** *17* (3), 195-211.
2. Portela, A.; Esteller, M., Epigenetic modifications and human disease. *Nature Biotechnology* **2010,** *28* (10), 1057-1068.
3. Chakrabarti, A.; Melesina, J.; Kolbinger, F. R.; Oehme, I.; Senger, J.; Witt, O.; Sippl, W.; Jung, M., Targeting histone deacetylase 8 as a therapeutic approach to cancer and neurodegenerative diseases. *Future Medicinal Chemistry* **2016,** *8* (13), 1609-1634.
4. Hu, E.; Chen, Z.; Fredrickson, T.; Zhu, Y.; Kirkpatrick, R.; Zhang, G.-F.; Johanson, K.; Sung, C.-M.; Liu, R.; Winkler, J., Cloning and Characterization of a Novel Human Class I Histone Deacetylase That Functions as a Transcription Repressor. *Journal of Biological Chemistry* **2000,** *275* (20), 15254-15264.

5. Singh, B. N.; Zhang, G.; Hwa, Y. L.; Li, J.; Dowdy, S. C.; Jiang, S.-W., Nonhistone protein acetylation as cancer therapy targets. *Expert Review of Anticancer Therapy* **2010,** *10* (6), 935-954.
6. Marks, P. A.; Rifkind, R. A.; Richon, V. M.; Breslow, R.; Miller, T.; Kelly, W. K., Histone deacetylases and cancer: causes and therapies. *Nature Reviews Cancer* **2001,** *1* (3), 194-202.
7. West, A. C.; Johnstone, R. W., New and emerging HDAC inhibitors for cancer treatment. *The Journal of Clinical Investigation* **2014,** *124* (1), 30-39.
8. Li, Y.; Seto, E., HDACs and HDAC Inhibitors in Cancer Development and Therapy. *Cold Spring Harbor Perspectives in Medicine* **2016,** *6* (10).
9. Wilson, A. J.; Byun, D.-S.; Popova, N.; Murray, L. B.; L'Italien, K.; Sowa, Y.; Arango, D.; Velcich, A.; Augenlicht, L. H.; Mariadason, J. M., Histone Deacetylase 3 (HDAC3) and Other Class I HDACs Regulate Colon Cell Maturation and p21 Expression and Are Deregulated in Human Colon Cancer. *Journal of Biological Chemistry* **2006,** *281* (19), 13548-13558.
10. Damaskos, C.; Tomos, I.; Garmpis, N.; Karakatsani, A.; Dimitroulis, D.; Garmpi, A.; Spartalis, E.; Kampolis, C. F.; Tsagkari, E.; Loukeri, A. A.; Margonis, G.-A.; Spartalis, M.; Andreatos, N.; Schizas, D.; Kokkineli, S.; Antoniou, E. A.; Nonni, A.; Tsourouflis, G.; Markatos, K.; Kontzoglou, K.; Kostakis, A.; Tomos, P., Histone Deacetylase Inhibitors as a Novel Targeted Therapy Against Non-small Cell Lung Cancer: Where Are We Now and What Should We Expect? *Anticancer Research* **2018,** *38* (1), 37-43.
11. Lehmann, A.; Denkert, C.; Budczies, J.; Buckendahl, A.-C.; Darb-Esfahani, S.; Noske, A.; Müller, B. M.; Bahra, M.; Neuhaus, P.; Dietel, M.; Kristiansen, G.; Weichert, W., High class I HDAC activity and expression are associated with RelA/p65 activation in pancreatic cancer in vitro and in vivo. *BMC Cancer* **2009,** *9* (1), 395.
12. Oehme, I.; Deubzer, H. E.; Wegener, D.; Pickert, D.; Linke, J.-P.; Hero, B.; Kopp-Schneider, A.; Westermann, F.; Ulrich, S. M.; von Deimling, A.; Fischer, M.; Witt, O., Histone Deacetylase 8 in Neuroblastoma Tumorigenesis. *Clinical Cancer Research* **2009,** *15* (1), 91-99.
13. Heimburg, T.; Kolbinger, F. R.; Zeyen, P.; Ghazy, E.; Herp, D.; Schmidtkunz, K.; Melesina, J.; Shaik, T. B.; Erdmann, F.; Schmidt, M.; Romier, C.; Robaa, D.; Witt, O.; Oehme, I.; Jung, M.; Sippl, W., Structure-Based Design and Biological Characterization of Selective Histone Deacetylase 8 (HDAC8) Inhibitors with Anti-Neuroblastoma Activity. *Journal of Medicinal Chemistry* **2017,** *60* (24), 10188-10204.
14. Rettig, I.; Koeneke, E.; Trippel, F.; Mueller, W. C.; Burhenne, J.; Kopp-Schneider, A.; Fabian, J.; Schober, A.; Fernekorn, U.; von Deimling, A.; Deubzer, H. E.; Milde, T.; Witt, O.; Oehme, I., Selective inhibition of HDAC8 decreases neuroblastoma growth in vitro and in vivo and enhances retinoic acid-mediated differentiation. *Cell Death & Disease* **2015,** *6* (2), e1657-e1657.
15. Tian, Y.; Wong, V. W. S.; Wong, G. L. H.; Yang, W.; Sun, H.; Shen, J.; Tong, J. H. M.; Go, M. Y. Y.; Cheung, Y. S.; Lai, P. B. S.; Zhou, M.; Xu, G.; Huang, T. H. M.; Yu, J.; To, K. F.; Cheng, A. S. L.; Chan, H. L. Y., Histone Deacetylase HDAC8 Promotes Insulin Resistance and β-Catenin Activation in NAFLD-Associated Hepatocellular Carcinoma. *Cancer Research* **2015,** *75* (22), 4803-4816.
16. Yang, W.; Feng, Y.; Zhou, J.; Cheung, O. K.-W.; Cao, J.; Wang, J.; Tang, W.; Tu, Y.; Xu, L.; Wu, F.; Tan, Z.; Sun, H.; Tian, Y.; Wong, J.; Lai, P. B.-S.; Chan, S. L.; Chan, A. W.-H.; Tan, P. B.-O.; Chen, Z.; Sung, J. J.-Y.; Yip, K. Y.-L.; To, K.-F.; Cheng, A. S.-L., A selective HDAC8 inhibitor potentiates antitumor immunity and efficacy of immune checkpoint blockade in hepatocellular carcinoma. *Science Translational Medicine* **2021,** *13* (588), eaaz6804.
17. Zhang, Q.; Wang, S.; Chen, J.; Yu, Z., Histone Deacetylases (HDACs) Guided Novel Therapies for T-cell lymphomas. *International Journal of Medical Sciences* **2019,** *16* (3), 424-442.
18. Kaufman, J. L.; Fabre, C.; Lonial, S.; Richardson, P. G., Histone Deacetylase Inhibitors in Multiple Myeloma: Rationale and Evidence for Their Use in Combination Therapy. *Clinical Lymphoma Myeloma and Leukemia* **2013,** *13* (4), 370-376.
19. Chuang, D.-M.; Leng, Y.; Marinova, Z.; Kim, H.-J.; Chiu, C.-T., Multiple roles of HDAC inhibition in neurodegenerative conditions. *Trends in Neurosciences* **2009,** *32* (11), 591-601.
20. Barton, K. M.; Archin, N. M.; Keedy, K. S.; Espeseth, A. S.; Zhang, Y.-l.; Gale, J.; Wagner, F. F.; Holson, E. B.; Margolis, D. M., Selective HDAC Inhibition for the Disruption of Latent HIV-1 Infection. *PLOS ONE* **2014,** *9* (8), e102684.
21. Nguyen, T. T. T.; Zhang, Y.; Shang, E.; Shu, C.; Torrini, C.; Zhao, J.; Bianchetti, E.; Mela, A.; Humala, N.; Mahajan, A.; Harmanci, A. O.; Lei, Z.; Maienschein-Cline, M.; Quinzii, C. M.; Westhoff, M.-A.; Karpel-Massler, G.; Bruce, J. N.; Canoll, P.; Siegelin, M. D., HDAC inhibitors elicit metabolic reprogramming by targeting super-enhancers in glioblastoma models. *The Journal of Clinical Investigation* **2020,** *130* (7), 3699-3716.
22. Chen, X.; Barozzi, I.; Termanini, A.; Prosperini, E.; Recchiuti, A.; Dalli, J.; Mietton, F.; Matteoli, G.; Hiebert, S.; Natoli, G., Requirement for the histone deacetylase Hdac3 for the

inflammatory gene expression program in macrophages. *Proceedings of the National Academy of Sciences* **2012,** *109* (42), E2865-E2874.
23. Giannini, G.; Cabri, W.; Fattorusso, C.; Rodriquez, M., Histone deacetylase inhibitors in the treatment of cancer: overview and perspectives. *Future Medicinal Chemistry* **2012,** *4* (11), 1439-1460.
24. Yoo, C. B.; Jones, P. A., Epigenetic therapy of cancer: past, present and future. *Nature Reviews Drug Discovery* **2006,** *5* (1), 37-50.
25. Marks, P. A.; Richon, V. M.; Rifkind, R. A., Histone Deacetylase Inhibitors: Inducers of Differentiation or Apoptosis of Transformed Cells. *JNCI: Journal of the National Cancer Institute* **2000,** *92* (15), 1210-1216.
26. Eckschlager, T.; Plch, J.; Stiborova, M.; Hrabeta, J., Histone Deacetylase Inhibitors as Anticancer Drugs. *International Journal of Molecular Sciences* **2017,** *18* (7), 1414.
27. Ho, T. C. S.; Chan, A. H. Y.; Ganesan, A., Thirty Years of HDAC Inhibitors: 2020 Insight and Hindsight. *Journal of Medicinal Chemistry* **2020,** *63* (21), 12460-12484.
28. Balasubramanian, S.; Ramos, J.; Luo, W.; Sirisawad, M.; Verner, E.; Buggy, J. J., A novel histone deacetylase 8 (HDAC8)-specific inhibitor PCI-34051 induces apoptosis in T-cell lymphomas. *Leukemia* **2008,** *22* (5), 1026-1034.
29. Lechner, S.; Malgapo, M. I. P.; Grätz, C.; Steimbach, R. R.; Baron, A.; Rüther, P.; Nadal, S.; Stumpf, C.; Loos, C.; Ku, X.; Prokofeva, P.; Lautenbacher, L.; Heimburg, T.; Würf, V.; Meng, C.; Wilhelm, M.; Sippl, W.; Kleigrewe, K.; Pauling, J. K.; Kramer, K.; Miller, A. K.; Pfaffl, M. W.; Linder, M. E.; Kuster, B.; Médard, G., Target deconvolution of HDAC pharmacopoeia reveals MBLAC2 as common off-target. *Nature Chemical Biology* **2022**.
30. Shen, S.; Kozikowski, A. P., Why Hydroxamates May Not Be the Best Histone Deacetylase Inhibitors—What Some May Have Forgotten or Would Rather Forget? *ChemMedChem* **2016,** *11* (1), 15-21.
31. Kang, S. P.; Ramirez, J.; House, L.; Zhang, W.; Mirkov, S.; Liu, W.; Haverfield, E.; Ratain, M. J., A pharmacogenetic study of vorinostat glucuronidation. *Pharmacogenetics and Genomics* **2010,** *20* (10), 638-641.
32. Wang, L.-Z.; Ramírez, J.; Yeo, W.; Chan, M.-Y. M.; Thuya, W.-L.; Lau, J.-Y. A.; Wan, S.-C.; Wong, A. L.-A.; Zee, Y.-K.; Lim, R.; Lee, S.-C.; Ho, P. C.; Lee, H.-S.; Chan, A.; Ansher, S.; Ratain, M. J.; Goh, B.-C., Glucuronidation by UGT1A1 Is the Dominant Pathway of the Metabolic Disposition of Belinostat in Liver Cancer Patients. *PLOS ONE* **2013,** *8* (1), e54522.
33. Du, L.; Musson, D. G.; Wang, A. Q., Stability studies of vorinostat and its two metabolites in human plasma, serum and urine. *Journal of Pharmaceutical and Biomedical Analysis* **2006,** *42* (5), 556-564.
34. Melesina, J.; Simoben, C. V.; Praetorius, L.; Bülbül, E. F.; Robaa, D.; Sippl, W., Strategies To Design Selective Histone Deacetylase Inhibitors. *ChemMedChem* **2021,** *16* (9), 1336-1359.
35. Jiang, Y.; Xu, J.; Yue, K.; Huang, C.; Qin, M.; Chi, D.; Yu, Q.; Zhu, Y.; Hou, X.; Xu, T.; Li, M.; Chou, C. J.; Li, X., Potent Hydrazide-Based HDAC Inhibitors with a Superior Pharmacokinetic Profile for Efficient Treatment of Acute Myeloid Leukemia In Vivo. *Journal of Medicinal Chemistry* **2022,** *65* (1), 285-302.
36. Wang, Y.; Stowe, Ryan L.; Pinello, Christie E.; Tian, G.; Madoux, F.; Li, D.; Zhao, Lisa Y.; Li, J.-L.; Wang, Y.; Wang, Y.; Ma, H.; Hodder, P.; Roush, William R.; Liao, D., Identification of Histone Deacetylase Inhibitors with Benzoylhydrazide Scaffold that Selectively Inhibit Class I Histone Deacetylases. *Chemistry & Biology* **2015,** *22* (2), 273-284.
37. McClure, J. J.; Zhang, C.; Inks, E. S.; Peterson, Y. K.; Li, J.; Chou, C. J., Development of Allosteric Hydrazide-Containing Class I Histone Deacetylase Inhibitors for Use in Acute Myeloid Leukemia. *Journal of Medicinal Chemistry* **2016,** *59* (21), 9942-9959.
38. Li, X.; Peterson, Y. K.; Inks, E. S.; Himes, R. A.; Li, J.; Zhang, Y.; Kong, X.; Chou, C. J., Class I HDAC Inhibitors Display Different Antitumor Mechanism in Leukemia and Prostatic Cancer Cells Depending on Their p53 Status. *Journal of Medicinal Chemistry* **2018,** *61* (6), 2589-2603.
39. Li, X.; Jiang, Y.; Peterson, Y. K.; Xu, T.; Himes, R. A.; Luo, X.; Yin, G.; Inks, E. S.; Dolloff, N.; Halene, S.; Chan, S. S. L.; Chou, C. J., Design of Hydrazide-Bearing HDACIs Based on Panobinostat and Their p53 and FLT3-ITD Dependency in Antileukemia Activity. *Journal of Medicinal Chemistry* **2020,** *63* (10), 5501-5525.
40. Chen, Y.; Zhang, L.; Zhang, L.; Jiang, Q.; Zhang, L., Discovery of indole-3-butyric acid derivatives as potent histone deacetylase inhibitors. *Journal of Enzyme Inhibition and Medicinal Chemistry* **2021,** *36* (1), 425-436.
41. Chakrabarti, A.; Oehme, I.; Witt, O.; Oliveira, G.; Sippl, W.; Romier, C.; Pierce, R. J.; Jung, M., HDAC8: a multifaceted target for therapeutic interventions. *Trends in Pharmacological Sciences* **2015,** *36* (7), 481-492.

42. Xiao, Y.; Wang, J.; Zhao, L. Y.; Chen, X.; Zheng, G.; Zhang, X.; Liao, D., Discovery of histone deacetylase 3 (HDAC3)-specific PROTACs. *Chemical Communications* **2020,** *56* (68), 9866-9869.
43. Kutil, Z.; Mikešová, J.; Zessin, M.; Meleshin, M.; Nováková, Z.; Alquicer, G.; Kozikowski, A.; Sippl, W.; Bařinka, C.; Schutkowski, M., Continuous Activity Assay for HDAC11 Enabling Reevaluation of HDAC Inhibitors. *ACS Omega* **2019,** *4* (22), 19895-19904.
44. Zessin, M.; Kutil, Z.; Meleshin, M.; Nováková, Z.; Ghazy, E.; Kalbas, D.; Marek, M.; Romier, C.; Sippl, W.; Bařinka, C.; Schutkowski, M., One-Atom Substitution Enables Direct and Continuous Monitoring of Histone Deacylase Activity. *Biochemistry* **2019,** *58* (48), 4777-4789.
45. Son, S. I.; Cao, J.; Zhu, C.-L.; Miller, S. P.; Lin, H., Activity-Guided Design of HDAC11-Specific Inhibitors. *ACS Chemical Biology* **2019,** *14* (7), 1393-1397.
46. Fu, Y.; Zhang, P.; Ge, J.; Cheng, J.; Dong, W.; Yuan, H.; Du, Y.; Yang, M.; Sun, R.; Jiang, H., Histone deacetylase 8 suppresses osteogenic differentiation of bone marrow stromal cells by inhibiting histone H3K9 acetylation and RUNX2 activity. *The International Journal of Biochemistry & Cell Biology* **2014,** *54*, 68-77.
47. Ferreira, R. C.; Popova, E. Y.; James, J.; Briones, M. R. S.; Zhang, S. S.; Barnstable, C. J., Histone Deacetylase 1 Is Essential for Rod Photoreceptor Differentiation by Regulating Acetylation at Histone H3 Lysine 9 and Histone H4 Lysine 12 in the Mouse Retina*. *Journal of Biological Chemistry* **2017,** *292* (6), 2422-2440.
48. Ji, H.; Zhou, Y.; Zhuang, X.; Zhu, Y.; Wu, Z.; Lu, Y.; Li, S.; Zeng, Y.; Lu, Q. R.; Huo, Y.; Shi, Y.; Bu, H., HDAC3 Deficiency Promotes Liver Cancer through a Defect in H3K9ac/H3K9me3 Transition. *Cancer Research* **2019,** *79* (14), 3676-3688.
49. Deardorff, M. A.; Bando, M.; Nakato, R.; Watrin, E.; Itoh, T.; Minamino, M.; Saitoh, K.; Komata, M.; Katou, Y.; Clark, D.; Cole, K. E.; De Baere, E.; Decroos, C.; Di Donato, N.; Ernst, S.; Francey, L. J.; Gyftodimou, Y.; Hirashima, K.; Hullings, M.; Ishikawa, Y.; Jaulin, C.; Kaur, M.; Kiyono, T.; Lombardi, P. M.; Magnaghi-Jaulin, L.; Mortier, G. R.; Nozaki, N.; Petersen, M. B.; Seimiya, H.; Siu, V. M.; Suzuki, Y.; Takagaki, K.; Wilde, J. J.; Willems, P. J.; Prigent, C.; Gillessen-Kaesbach, G.; Christianson, D. W.; Kaiser, F. J.; Jackson, L. G.; Hirota, T.; Krantz, I. D.; Shirahige, K., HDAC8 mutations in Cornelia de Lange syndrome affect the cohesin acetylation cycle. *Nature* **2012,** *489* (7415), 313-317.
50. Borst, J.; Ahrends, T.; Bąbała, N.; Melief, C. J. M.; Kastenmüller, W., CD4+ T cell help in cancer immunology and immunotherapy. *Nature Reviews Immunology* **2018,** *18* (10), 635-647.
51. Kutil, Z.; Novakova, Z.; Meleshin, M.; Mikesova, J.; Schutkowski, M.; Barinka, C., Histone Deacetylase 11 Is a Fatty-Acid Deacylase. *ACS Chemical Biology* **2018,** *13* (3), 685-693.
52. Ibrahim, H. S.; Abdelsalam, M.; Zeyn, Y.; Zessin, M.; Mustafa, A.-H. M.; Fischer, M. A.; Zeyen, P.; Sun, P.; Bülbül, E. F.; Vecchio, A.; Erdmann, F.; Schmidt, M.; Robaa, D.; Barinka, C.; Romier, C.; Schutkowski, M.; Krämer, O. H.; Sippl, W., Synthesis, Molecular Docking and Biological Characterization of Pyrazine Linked 2-Aminobenzamides as New Class I Selective Histone Deacetylase (HDAC) Inhibitors with Anti-Leukemic Activity. *International Journal of Molecular Sciences* **2022,** *23* (1), 369.
53. Zhou, J.; Liu, M.; Sun, H.; Feng, Y.; Xu, L.; Chan, A. W. H.; Tong, J. H.; Wong, J.; Chong, C. C. N.; Lai, P. B. S.; Wang, H. K.-S.; Tsang, S.-W.; Goodwin, T.; Liu, R.; Huang, L.; Chen, Z.; Sung, J. J.; Chow, K. L.; To, K. F.; Cheng, A. S.-L., Hepatoma-intrinsic CCRK inhibition diminishes myeloid-derived suppressor cell immunosuppression and enhances immune-checkpoint blockade efficacy. *Gut* **2018,** *67* (5), 931-944.